



**Sinking aggregates**

T. Jokulsdottir and  
D. Archer

# A Stochastic, Lagrangian Model of Sinking biogenic aggregates in the ocean (SLAMS 1.0): model formulation, validation and sensitivity

T. Jokulsdottir and D. Archer

University of Chicago, Chicago, IL 60637, USA

Received: 21 May 2015 – Accepted: 20 June 2015 – Published: 28 July 2015

Correspondence to: T. Jokulsdottir (tinnsi@gmail.com)

Published by Copernicus Publications on behalf of the European Geosciences Union.

Title Page

Abstract

Introduction

Conclusions

References

Tables

Figures



Back

Close

Full Screen / Esc

Printer-friendly Version

Interactive Discussion



## Abstract

We present a new mechanistic model, Stochastic Lagrangian Aggregate Model of Sinking particles (SLAMS) for the biological pump in the ocean, which tracks the evolution of individual particles as they aggregate, disaggregate, sink, and are altered by chemical and biological processes. SLAMS considers the impacts of ballasting by mineral phases, binding of aggregates by transparent exopolymer particles (TEP), zooplankton grazing, and the fractal geometry (porosity) of the aggregates. Parameterizations for age-dependent organic carbon (orgC) degradation kinetics, and disaggregation driven by zooplankton grazing and TEP degradation, are motivated by observed particle fluxes and size spectra throughout the water column. The model is able to explain observed variations in orgC export efficiency and rain ratio from the euphotic zone and to the sea floor as driven by sea surface temperature and the primary production rate and seasonality of primary production. The model provides a new mechanistic framework with which to predict future changes on the flux attenuation of orgC in response to climate change forcing.

## 1 Introduction

Plankton in the ocean incorporate dissolved carbon and nutrients into particulate form (cells, marine snow and fecal pellets), which allows the constituents to sink through the water column until the particles decompose at depth. This process, called the biological pump (Ducklow et al., 2001; Buesseler et al., 2008), results in a major rearrangement of the chemistry of the oceans. The  $\text{CO}_2$  concentration in the atmosphere is coupled with the chemistry of the surface ocean, giving the biological pump a hand in controlling atmospheric  $\text{CO}_2$  and the climate of the Earth (Schneider et al., 2008; Kwon et al., 2009). One major uncertainty in future climate change projections is the response of the biological pump in the ocean to surface ocean conditions (thermal and chemical) (Friedlingstein et al., 2001). Here we develop a new numerical model, SLAMS, to simu-

GMDD

8, 5931–5982, 2015

## Sinking aggregates

T. Jokulsdottir and  
D. Archer

Title Page

Abstract

Introduction

Conclusions

References

Tables

Figures

◀

▶

◀

▶

Back

Close

Full Screen / Esc

Printer-friendly Version

Interactive Discussion



late the processes and characteristics of sinking particles in the ocean, to gain a better understanding of what factors affect the flux of orgC, and how it might respond to changing upper ocean chemistry and climate.

Particles in the ocean span about 5 orders of magnitude in size and 15 orders of magnitude in number density. Measurements have shown that the majority of the flux is composed of slow ( $< 10 \text{ mday}^{-1}$ ) and fast ( $> 350 \text{ mday}^{-1}$ ) sinking particles (Riley et al., 2012; Alonso-Gonzalez et al., 2010). We consider two types of particle formation: aggregation of particles (also called marine snow) and grazing and packaging by zooplankton producing fecal pellets.

Flux attenuation of sinking organic particles is determined by the sinking velocity of particles and the rate of orgC respiration. Sinking velocity generally increases with particle size and density (Alldredge and Gotschalk, 1988; Ploug et al., 2008) and it has also been found to increase with depth, driven by evolution of particle size or density (Berelson, 2002). Normalized POC flux to mass flux shows that orgC comprises about 5% of the mass flux in the deep ocean (Armstrong et al., 2002). The near constancy of this ratio suggests that ballasting (we use the term ballast to discuss the increase in density by biominerals) by minerals plays a key role in determining the orgC sinking flux (Klaas and Archer, 2002; Francois et al., 2002; Boyd and Trull, 2007). On the other hand, minerals are not inherently sticky, and an overabundance of mineral particles relative to TEP in laboratory experiments has been found to decrease the sizes of the aggregates (Passow and De La Rocha, 2006), which could act to diminish the sinking flux.

Biologically and chemically driven processes act on particles to change their physical and chemical structure. The respiration of organic matter by bacteria is a complex, sequential process (Biddanda and Pomeroy, 1988), as indicated by an observed correlation between the degradation rate of orgC and its age, spanning 8 orders of magnitude (Emerson and Hedges, 1988; Hedges and Keil, 1995). Association with mineral surfaces also acts to protect orgC from enzymatic degradation (Engel, 2009; Moigne et al., 2013). Three processes take place in zooplankton guts: respiration of

## Sinking aggregates

T. Jokulsdottir and  
D. Archer

Title Page

Abstract

Introduction

Conclusions

References

Tables

Figures

I◀

▶I

◀

▶

Back

Close

Full Screen / Esc

Printer-friendly Version

Interactive Discussion



## Sinking aggregates

T. Jokulsdottir and  
D. Archer

Title Page

Abstract

Introduction

Conclusions

References

Tables

Figures

I ◀

▶ I

◀

▶

Back

Close

Full Screen / Esc

Printer-friendly Version

Interactive Discussion



orgC, dissolution of calcium carbonate, and repackaging of phytoplankton cells into fecal pellets. Fecal pellets that are packaged more tightly than aggregated marine snow have a potential to sink quickly through the water column. Aggregate fragmentation is driven by zooplankton swimming and feeding (Alldredge et al., 1990) and the bacterial breakdown of TEP which leaves aggregates un-sticky and prone to break up (Passow and De La Rocha, 2006). In addition to biological dissolution of  $\text{CaCO}_3$  in zooplankton guts, there appears to be significant dissolution of the more soluble  $\text{CaCO}_3$  mineral aragonite in the water column (Gangsto et al., 2008). Biogenic silica, the other main biomineral in the ocean, is undersaturated throughout the ocean, and is distinguished by a strong temperature sensitivity of its dissolution rate, dissolving significantly faster in warm waters (Gnanadesikan, 1999).

The goal of this study is to formulate a numerical model intended to simulate these physio-bio-chemical dynamics. Observed flux from sediment traps in the Equatorial Pacific is used as a study site to tune parameters that are ad hoc or unknown. Model flux is compared to observed flux in the deep, pe-ratio (the fraction of produced organic carbon that is exported) and the rain ratio ( $\text{orgC}/\text{CaCO}_3$ ) at the seafloor is compared to data. We are interested in understanding the effects of changing a climatic parameter on the attenuation of the orgC flux. Finally we look at the sensitivity of the model to sea surface temperatures (SSTs), primary production (PP) and a bloom index (BI) which is a measure of seasonality.

## 2 Model description

We have developed a model, SLAMS, that simulates the flux of orgC and minerals through the water column from the sea surface where production of particles takes place to the seafloor at 4 km depth. The most common approach to modeling the flux of material through the water column is using a spectrum of particle size classes that aggregate according to coagulation theory, based on the sectional method of (Jackson, 1990). In a sectional model, particles are binned according to size and other charac-

## Sinking aggregates

T. Jokulsdottir and  
D. Archer[Title Page](#)[Abstract](#)[Introduction](#)[Conclusions](#)[References](#)[Tables](#)[Figures](#)[I◀](#)[▶I](#)[◀](#)[▶](#)[Back](#)[Close](#)[Full Screen / Esc](#)[Printer-friendly Version](#)[Interactive Discussion](#)

teristics and the concentration of particles in each bin is the prognostic variable. The transfer of material between size bins by aggregation and fragmentation is calculated using the Smoluchowski equation. This model is able to reproduce the slope of the particle size spectrum (log of number spectrum plotted against log of the particle radius) typically found in marine environments (Jackson, 1990, 1995). Here we simulate Lagrangian particles using a modified super particle method described in this section. The advantage gained by the Lagrangian approach is that we can track a large number of aggregate compositions (orgC and minerals).

## 2.1 Aggregate classes

The constitutive elements of SLAMS are the aggregates. They are clusters of *primary particles*, a combination of phytoplankton cells (coccolithophorids, diatoms, picoplankton), TEP particles, and terrigenous dust particles. SLAMS keeps track of a large number of aggregates that we call aggregate classes (AC). Each AC carries a suite of information about the state of one class of aggregate in the water column (Table 1). Aggregate classes, also called super-particles or super-droplets in atmospheric applications, are representative of some variable number,  $n$ , of identical aggregates (Sect. 2.3.1). Each aggregate is composed of  $p$  primary particles (Fig. 1), forming an aggregate consisting of up to 10 types of orgC (representing different ages), up to 10 types of TEP (also representing different ages), and four types of minerals (calcite, aragonite, biogenic silica, and terrigenous material). Lability of orgC and TEP is determined from its age. From this information, SLAMS constructs the physical characteristics of the aggregate that determine its sinking velocity.

## 2.2 Production

20 new ACs are created per 8 h time step within the euphotic zone in the model. This number is a trade-off between computation time and smoothness of the runs – 20 per time step turned out to be more than enough ACs to provide consistent results

## Sinking aggregates

T. Jokulsdottir and  
D. Archer

Title Page

Abstract

Introduction

Conclusions

References

Tables

Figures

I ◀

▶ I

◀

▶

Back

Close

Full Screen / Esc

Printer-friendly Version

Interactive Discussion



between runs and an acceptable run-time. The type of phytoplankton (or terrigenous material) of each new particle is chosen by a Monte Carlo method, wherein a uniformly distributed random number between 0 and 1 is generated and compared with ranges in Table 3. Table 3 shows the default functional group in SLAMS that is a typical open ocean assemble and would require modification with information on specific functional types and rates of particle production for detailed regional applications. When an AC is produced,  $p = 1$ , meaning that the AC represents many copies of a single cell (primary particle) that has not aggregated. The default settings are those of the Equatorial Pacific, where primary production is  $1000 \text{ mg C m}^{-2} \text{ d}^{-1}$ , so each AC (unless it is terrigenous material) therefore initially contains  $1000/20 \cdot 8/24 = 16.7 \text{ mg C}$  or  $1.39 \text{ mmol C}$ . The amount of orgC per phytoplankton cell determines the number of primary particles ( $n$ ) that the AC will initially represent (Table 3). For example, a coccolithophorid in our model contains  $7 \text{ pmol orgC}$ . If the random number generated indicates production of coccolithophorids,  $n = 1.39 \times 10^{-3} / 7 \times 10^{-12} = 1.98 \times 10^8$  coccolithophorids. The default functional groups (Table 3) are used for all regions, except the Southern Ocean where calcifiers produce half as much calcium carbonate and diatoms produce twice as much biogenic silica as in the rest of the simulations.

The kinetics of particle aggregation depend on the encounter rate and the probability of sticking (stickiness =  $\alpha$  = interparticle attachment rate/interparticle collision rate) (Allredge and McGillivray, 1991). The main glue that holds marine snow together in the water column appears to be transparent exopolymer particles (TEP), a mucus-like polysaccharide material exuded by phytoplankton and bacteria, especially under conditions of nutrient limitation during the senescent phase of phytoplankton blooms (Engel, 2000; Logan et al., 1995; Dam and Drapeau, 1995; Kahl et al., 2008). It is exuded in dissolved form but it separates into suspended droplets, or gel, in conditions of turbulence (Verdugo et al., 2004). In SLAMS, TEP production consists of 6% of the primary production in the default case, in terms of carbon. This number comes from sensitivity studies where we simulate Equatorial Pacific conditions (SST, PP and seasonality) and compare orgC flux to the deep ocean to sediment trap data. In the model

## Sinking aggregates

T. Jokulsdottir and  
D. Archer

Title Page

Abstract

Introduction

Conclusions

References

Tables

Figures

I◀

▶I

◀

▶

Back

Close

Full Screen / Esc

Printer-friendly Version

Interactive Discussion



formulation TEP is not part of primary production but an independent variable that can be changed without altering primary production allowing for sensitivity analysis of TEP. In each timestep, 20 new ACs are produced that are phytoplankton or terrigenous material, and 1 new aggregate that is TEP. In the default case 6% of primary production (1000 mgC m<sup>-2</sup> d<sup>-1</sup>) is 60 mgC m<sup>-2</sup> d<sup>-1</sup>. One TEP particle contains 1 pmol carbon and so  $n = 5 \times 10^9$ . The role of TEP in controlling the flux of organic matter is complicated however by its low density ( $\sim 0.8 \text{ g cm}^{-3}$ ), which acts to decrease the overall density of an aggregate, potentially to the point where it becomes buoyant and ascends rather than sinks (Mari, 2008). The density of TEP is less than the density of sea water which results in a possible upward ascend of particles. Upward movement is allowed in the model. It prompted us to consider what happens to buoyant particles at the sea surface and include photolysis in the model.

## 2.3 Aggregation

### 2.3.1 Rate of aggregation

The rate of particle aggregation is governed by two limiting mechanisms: the rate of collision ( $\beta$ ) (see discussion in eg. Jackson, 1995; Burd and Jackson, 1997, 2009) and the rate of sticking ( $\alpha$ ) once collided. As described above, much of the stickiness of aggregates appears to be due to TEP (Alldredge et al., 1995; Engel, 2000; Verdugo et al., 2004). Our formulation for particle stickiness is simple, in that TEP particles have  $\alpha = 1$  and at the time of production the stickiness of all other particles is 0. After a particle aggregates, its stickiness is the volume-weighted average of the stickiness of the component particles:

$$\alpha = \frac{V_{\text{TEP}}}{V_a}, \quad (1)$$

where  $V_{\text{TEP}}$  is the volume of TEP in the aggregate and  $V_a$  is the volume of the entire aggregate, represents how likely two colloids or aggregates are to stick if they collide

and ranges from 0 to 1. As a result, in SLAMS, particles do not stick unless TEP is present.

Particles collide by three mechanisms; very small particles mostly encounter each other by Brownian motion, whereas large particles meet most of their partners due to fluid shear and differential settling (the larger particle settling faster and sweeping up the smaller ones). In SLAMS, the coagulation kernel  $\beta$  is a sum of three mechanisms: Collision frequency due to Brownian motion:

$$\beta_{\text{Br}} = \frac{8kT}{6\mu} \frac{(r_i + r_j)^2}{r_i r_j}, \quad (2)$$

shear:

$$\beta_{\text{sh}} = 9.8 \frac{q^2}{1 + 2q^2} \sqrt{\left(\frac{\varepsilon}{\nu}\right)} (r_i + r_j)^3 \quad (3)$$

where

$$q = \text{MIN}(r_i, r_j) / \text{MAX}(r_i, r_j) \quad (4)$$

and differential settling:

$$\beta_{\text{ds}} = \frac{1}{2} \pi \text{MIN}(r_i, r_j)^2 |u_i - u_j| \quad (5)$$

(Burd and Jackson, 1997, 2009). Here  $k$  is the Stefan–Boltzman constant,  $\mu$  is the dynamic viscosity,  $\nu$  is kinematic viscosity,  $\varepsilon$  is the turbulent dissipation rate set to  $1 \times 10^{-4}$ .  $r_i$  and  $r_j$  are the radii of the two aggregates being evaluated for collision and  $u_i$  and  $u_j$  are the settling velocities of the two aggregates.

## GMDD

8, 5931–5982, 2015

### Sinking aggregates

T. Jokulsdottir and  
D. Archer

Title Page

Abstract

Introduction

Conclusions

References

Tables

Figures

⏪

⏩

◀

▶

Back

Close

Full Screen / Esc

Printer-friendly Version

Interactive Discussion



### 2.3.2 Model formulation of aggregation

In the real world, in a given amount of time, some fraction of the particles represented by an AC in our scheme might aggregate with a particular other class of particles and others not. In order to prevent an unmanageable proliferation of particle types, we require that either all of the less-numerous particles find partners in a given time step, or none of them do. The decision is made stochastically using a Monte Carlo method. The idea is that over many possible aggregations, the overall behavior will be statistically similar to a real-world case, or a sectional model, where only a fraction of the particles would aggregate in any given time step. If instead we would allow a fraction of the aggregates in an AC to aggregate and not all of them, then a new AC would have to be made for every successful aggregation adding hundreds of new ACs each timestep. Figure 2 shows an example of two particles sticking. The main advantage of a stochastic over a deterministic approach to aggregation simulation is that here we are able to simulate a large number of compositions without altering the run time.

The number ( $\xi$ ) of ACs in a depth bin is variable, depending on aggregation and sinking rate. After the first timestep,  $\xi = 21$  in the top depth bin and after the second timestep  $\xi = 42$  unless one or more aggregates sank out. After the model has reached steady state,  $\xi$  is a few hundred or a few thousand, depending on the depth and conditions. Each time step, within each depth bin, we pick  $\xi(\xi - 1)/2$  pairs of ACs uniformly at random for potential aggregation. For a given pair, we denote the indices of the ACs by  $(i, j)$ , and assume that  $n_j \geq n_i$ , i.e. the number of aggregates in AC  $i$  is equal or smaller than the number of aggregates in AC  $j$ . For each such pair of aggregates, we compute the probability of aggregation between a single  $i$  aggregate and  $n_j$   $j$ -type aggregates as  $P_{i,j}$ :

$$P_{i,j} = \alpha(i, j)\beta(i, j)\frac{dt}{dV} \quad (6)$$

## Sinking aggregates

T. Jokulsdottir and  
D. Archer

Title Page

Abstract

Introduction

Conclusions

References

Tables

Figures

I◀

▶I

◀

▶

Back

Close

Full Screen / Esc

Printer-friendly Version

Interactive Discussion



where  $\alpha(i, j)$  and  $\beta(i, j)$  are the stickiness parameter and coagulation kernel respectively. Equation (6) represents a continuous time model. In SLAMS we approximate Eq. (6) by discretizing in time. As a result, for a given encounter where one of the aggregates is extremely large, it is possible that  $P_{i,j} > 1$ . We take a  $P_{i,j} > 1$  as an indication that the time step  $dt$  has been chosen to be too large for the approximation to be reasonable hence reducing  $dt$  is appropriate. In that case the time step is decreased by factors of 10 until  $P_{i,j} < 1$ .

We derive the expected number of aggregation events between all of the  $i$  and  $j$  aggregates given by  $E_j$ : Assuming there are  $n_j$   $j$ -particles and  $n_i = 1$   $i$  particle and that the probability of aggregation,  $P$ , is constant, the expected number of aggregations in timestep  $dt$  is

$$E [q_1] = n_j \cdot P \quad (7)$$

where  $q_1$  is the number of aggregations the one  $i$  particle experiences. For  $n_i = 2$  we find the expected number of aggregations that the second  $i$  particle undergoes, conditional on  $q_1$ ,

$$E [q_2|q_1] = (n_j - q_1)P, \quad (8)$$

where  $q_2$  is the number of aggregations the second  $i$  particle experiences. The total number of aggregations that take place between  $i$  and  $j$  particles for  $n_i = 2$  is

$$E [q_1 + q_2] = E [n_j P + (n_j - q_1)P] = n_j P (1 + (1 - P)). \quad (9)$$

For  $n_i = 3$ ,

$$E [q_3|q_1, q_2] = (n_j - q_1 - q_2)P \quad (10)$$

and so the total number of aggregations when  $n_i = 3$  is:

$$E [q_1 + q_2 + q_3] = E [q_1 + q_2 + (n_j - q_1 - q_2)P]$$

$$\begin{aligned}
 &= n_j P + n_j P(1 - P) + (n_j - n_j P - n_j P(1 - P))P \\
 &= n_j P + n_j P(1 - P) + n_j P(1 - P)(1 - P).
 \end{aligned}
 \tag{11}$$

By induction, we obtain the following general formula for the expected number of aggregations when  $n_j > n_i$

$$E \left[ \sum_{k=1}^{n_j} q_k \right] = n_j P \sum_{k=0}^{n_i-1} (1 - P)^k = n_j (1 - (1 - P)^{n_i}).
 \tag{12}$$

The mean number of  $j$ -particles that aggregate with a given  $i$  particle is therefore

$$E_j = \frac{n_j}{n_i} (1 - (1 - P)^{n_i}).
 \tag{13}$$

Assuming independence of particles, the variance is

$$\sigma^2 = \frac{n_j}{n_i} (1 - P)(1 - (1 - P)^{n_i}).
 \tag{14}$$

we round  $E_j$  to the nearest integer. If  $E_j > 0$ , aggregates will aggregate.  $E_j$   $j$ -aggregates stick to each  $i$ -aggregate. The AC that at the beginning of the timestep represented aggregate  $i$  now represents  $n_i$  aggregates with  $p = p_i + E_j \cdot p_j$ . The AC that was aggregate- $j$  is unchanged after the time step except that it now represents  $n = n_j - E_j \cdot n_i$  aggregates. The scheme was designed so that the number of ACs remains unchanged through a aggregation event. This prevents a runaway escalation of the computational load of the run.

## 2.4 Physical characteristics of aggregates

An aggregate that forms by aggregation of smaller particles forms a fractal structure with a dimension,  $D_N$ , that describes its porosity:  $\rho \sim r_a^{D_N}$  where  $\rho$  is the number of primary particles and  $r_a$  is the radius of the aggregate (Logan and Wilkinson, 1990). The

## Sinking aggregates

T. Jokulsdottir and  
D. Archer

Title Page

Abstract

Introduction

Conclusions

References

Tables

Figures

◀

▶

◀

▶

Back

Close

Full Screen / Esc

Printer-friendly Version

Interactive Discussion



## Sinking aggregates

T. Jokulsdottir and  
D. Archer

Title Page

Abstract

Introduction

Conclusions

References

Tables

Figures

I◀

▶I

◀

▶

Back

Close

Full Screen / Esc

Printer-friendly Version

Interactive Discussion



closer  $D_N$  is to 3, the more the structure fills up 3-dimensional space, and the lower its porosity. The fractal dimension of marine snow has been inferred from measurements of aggregate properties such as settling velocity, porosity, and size, to be in the range of 1.3 to 2.3 (Logan and Wilkinson, 1990; Li and Logan, 1995). The porosity of marine snow appears to be large, always above 0.9 and mostly closer to 0.99, increasing with the diameter of the aggregate (Alldredge and Silver, 1988; Ploug et al., 2008). Fecal pellets are more compact, and thus their porosity is smaller, about 0.43–0.65 (Ploug et al., 2008). The aggregate sinking velocity depends on the aggregate radius and porosity. We follow Logan and Wilkinson (1990) calculating radius and porosity from the fractal dimension and composition of the aggregate (Table 1). The fractal dimension of aggregates in SLAMS is  $D_N = 2.0$  (Li and Logan, 1995). Fecal pellets are not fractal in nature, so we use the relationship between fecal pellet volume and sinking rate developed by (Small et al., 1979) and find that a porosity of 0.5 results in sinking velocity of model pellets that compare well to that relationship. The resulting model pellet density for 0.5 porosity is near the range of measured pellet density of 1.08–1.2, depending on the composition of the pellet Ploug et al. (2008); Feinberg and Dam (1998). The aggregate radius,  $r_a$  is obtained from the fractal dimension and the radius of the primary particle,  $r_p$ :

$$r_a = r_p \cdot \rho^{1/D_N} \quad (15)$$

The radius of the primary particle,  $r_p$ , is calculated from its volume under the assumption that it is a perfect sphere:

$$r_p = \sqrt[3]{\frac{3V_p}{4\pi}} \quad (16)$$

where  $V_p$ , the volume of the primary particles in the aggregate, is calculated by dividing the total volume of material in the aggregate,  $V_m$ , by the number of primary particles:

$$V_p = \frac{V_m}{\rho} \quad (17)$$

And

$$V_m = \sum_{i=1}^5 X_i \cdot \frac{mw_i}{\rho_i} \quad (18)$$

where  $X_i$  is the concentration [mol] of substance  $i$ ,  $mw_i$  is its molar weight and  $\rho_i$  is its density.  $i \in [\sum \text{orgC}, \sum \text{TEP}, \text{CaCO}_3, \text{bSi}, \text{dust}]$ .

The porosity,  $\phi$ , is related to the volume of individual particles that makes up the aggregate to the total volume of the aggregate:

$$\phi = 1 - \frac{\rho \cdot V_p}{V_a} = 1 - \rho \left( \frac{r_p}{r_a} \right)^3 \quad (19)$$

where

$$V_a = \frac{4}{3} \pi r_a^3 \quad (20)$$

(Logan and Wilkinson, 1990). The density of the aggregate,  $\rho_a$ , is calculated from the density of the material in the aggregate,  $\rho_s$ , the density of seawater,  $\rho_{sw}$  and the porosity,  $\phi$ :

$$\rho_a = (1 - \phi)\rho_s + \rho_{sw}. \quad (21)$$

## 2.5 Settling

Sinking velocities of particles range from a few up to hundreds of meters per day (Trull et al., 2008) and have been found to increase with depth (Berelson, 2002). The sinking orgC flux of particles in the ocean, binned according to sinking velocity of the particles, has been found to exhibit a bimodal distribution, with substantial fluxes from particles sinking at about  $1 \text{ m d}^{-1}$ , and close to  $1000 \text{ m d}^{-1}$ , but very little in between suggesting

## Sinking aggregates

T. Jokulsdottir and  
D. Archer

Title Page

Abstract

Introduction

Conclusions

References

Tables

Figures

◀

▶

◀

▶

Back

Close

Full Screen / Esc

Printer-friendly Version

Interactive Discussion



there are two types of sinking particles that make up the orgC sinking flux (Alonso-Gonzalez et al., 2010; McDonnell and Buesseler, 2010). In SLAMS, the aggregate sinking velocity:

$$u = \sqrt{\frac{8r_a (\rho_a - \rho_{sw})g}{3\rho_{sw}f(Re)}}, \quad (22)$$

5 is calculated using Stokes' law (Alldredge and Gotschalk, 1988), where  $g$  is the gravity of earth. For low Reynolds numbers where viscous forces are dominant,

$$f(Re) = 24/Re \quad (23)$$

and

$$Re = 2r_a u / \nu \quad (24)$$

10 where  $\nu$  is kinematic viscosity. For large Reynolds numbers where turbulence starts to play a role, the drag coefficient is calculated using Whites' approximation:

$$f(Re) = 24/Re + 6/(1 + \sqrt{Re}) + 0.4 \quad (25)$$

(White, 1991), which is valid for  $Re < 2 \times 10^4$ . Substituting  $f(Re)$  with White's approximation results in a nonlinear equation with  $u$  as the variable which we solve for using  
 15 Newtons' method. Model aggregates only sink vertically, there are no lateral currents. Aggregates reach high  $Re$  conditions when settling at a few hundred meters per day, depending on their size.

Within the range of salinity found in the ocean, the viscosity of seawater is mainly a function of temperature (Dorsey, 1940). We use a formula that fits empirical data of  
 20 seawater viscosity at 35 ppt:

$$\nu = 5 \times 10^{-6} \exp(2250/T) \quad (26)$$

**Sinking aggregates**

T. Jokulsdottir and  
D. Archer

Title Page	
Abstract	Introduction
Conclusions	References
Tables	Figures
◀	▶
◀	▶
Back	Close
Full Screen / Esc	
Printer-friendly Version	
Interactive Discussion	



to find the viscosity,  $\nu$ , at temperature  $T$  [K]. The change in viscosity with temperature has a large effect on the sinking velocity of particles. For the change in sea water temperatures from the sea surface to the sea floor in the tropics, the change in viscosity leads to a 50 % decrease in sinking velocity.

## 2.6 Organic carbon and TEP degradation

Bacteria are relevant to the biological pump for their role in degradation of orgC. Organic carbon is a chemically heterogeneous combination of proteins, lignin and cellulose which vary in structure and degradability (Westrich and Berner, 1984), and as it degrades, its heterogeneity increases. As the structure is altered, it becomes increasingly unrecognizable to enzymes (Emerson and Hedges, 1988), producing the observed decrease in reactivity. TEP degradation is treated the same way as orgC degradation. Respiration rates have been measured, both on natural aggregates collected in the ocean, and on aggregates formed in laboratory roller tanks from freeze-killed diatom ooze. Higher respiration rates and bacterial production were found in younger (1–3 days) than in older (7–14 days) aggregates, as the labile proteins were respired first, leaving the less labile material to be respired more slowly (Grossart and Ploug, 2000). Observed respiration rates of fresh phytoplankton range between 0.057 and 0.089 d<sup>-1</sup> (Grossart and Ploug, 2001) or 0.083 ± 0.034 d<sup>-1</sup> (Ploug and Grossart, 2000), and generally decrease with time, from 0.09 initially to 0.05 d<sup>-1</sup> three days later (Grossart et al., 2003). Light energy has also been shown to break down dissolved orgC, especially refractory compounds (Mopper et al., 1991).

To simulate the decrease in degradation rate with orgC age, we track 10 age bins for orgC in each aggregate, and construct a degradation rate that is both a function of age and temperature:

$$d \text{orgC}_i = k(i, T) \cdot \text{orgC}_i dt \quad (27)$$

Title Page

Abstract

Introduction

Conclusions

References

Tables

Figures

◀

▶

◀

▶

Back

Close

Full Screen / Esc

Printer-friendly Version

Interactive Discussion



where  $l$  stands for the age bin and  $T$  is temperature [ $^{\circ}\text{C}$ ]. The age of the orgC in bin  $l$ ,  $\text{age}_l$ , is  $2^{l-2}$  to  $2^{l-1}$  days and

$$k(l, T) = 0.1 / \text{age}_l \cdot \exp(\ln 2(T - 30) / 10). \quad (28)$$

This relation assigns freshly produced orgC at the sea surface a degradation lifetime of a few days, and it prescribes a decrease in reaction rate with phytoplankton age (Grossart and Ploug, 2001; Ploug and Grossart, 2000; Grossart et al., 2003) following the observations of Middelburg (1989). The temperature dependence results in about a doubling of the reaction rate with  $10^{\circ}\text{C}$  of warming, a moderate activation energy of about  $45 \text{ kJ mol}^{-1}$ . Aging of orgC and TEP is accomplished by transferring orgC,  $dt / (\text{age}_l - \text{age}_{l-1})$  orgC (or TEP) from bin  $l$  into bin  $l + 1$  for  $l = 1, \dots, 9$ . Material does not age out of the top bin,  $l = 10$ .

If the fraction of TEP, the stickiness, of an aggregate is less than 0.02, it breaks into  $P_f$  fragments as described in Sect. 2.7.1.

## 2.7 Zooplankton

The presence of slowly-sinking small particles in the deep ocean attests to the effects of disaggregation or fragmentation of aggregates in the water column (Jackson, 1995). In a sectional modeling study, (Ruiz, 1997) treated disaggregation as driven by turbulent flow in the ocean. Laboratory experiments with diatom aggregates (a fragile form of marine snow) find that stresses in excess of those due to turbulent shear in the water column are required to break them, pointing to biological shear and grazing as the dominant breaking mechanism (Alldredge et al., 1990). The abundance of marine snow appears to undergo daily cycles (Lampitt et al., 1993; Stemmann et al., 2000), its concentration dropping at night coincident with increasing in zooplankton abundance (Graham et al., 2000). A positive correlation between zooplankton concentration and particle number density also supports a strong role for zooplankton fragmenting aggregates (Dilling and Alldredge, 2000).

## Sinking aggregates

T. Jokulsdottir and  
D. Archer

Title Page

Abstract

Introduction

Conclusions

References

Tables

Figures

◀

▶

◀

▶

Back

Close

Full Screen / Esc

Printer-friendly Version

Interactive Discussion



The zooplankton in our model have the ability to fragment and ingest aggregates and produce a range of fecal pellet sizes. However, the various constraints on the model dynamics arising from the observational data required a metabolic efficiency scaling factor,  $g(z)$ , that increases from the surface to about 400 m and then decreases again (Fig. 3).

We construct an encounter probability:

$$R_{\text{enc}} = Z \cdot g(z) dt \quad (29)$$

where

$$Z = \sum_{j=1}^{\xi} \sum_{l=1}^{10} \text{orgC}_{l,j} \quad (30)$$

is the amount of orgC in each depth-bin. For each AC, at each time step, a random number,  $r$ , is generated and compared to  $R_{\text{enc}}$ . If  $r < R_{\text{enc}}$ , the zooplankton do encounter the AC and either ingest it (all the real aggregates it represents) or fragment it.

### 2.7.1 Fragmentation

To determine whether the aggregates encountered by zooplankton are fragmented or ingested SLAMS first checks if it is fragmented. We assume the efficiency for breaking small particles is lower than for breaking large ones (Alldredge et al., 1990). We account for this relationship with a parameter,  $R_{\text{break}}$ , that increases with aggregate radius, so that it is more likely that zooplankton are able to break large aggregates than small, if they do encounter an aggregate. Again to satisfy particle spectrum data, we come up with the equation:

$$R_{\text{break}} = 0.1 \arctan \left( r_a / 10^4 \right). \quad (31)$$

## Sinking aggregates

T. Jokulsdottir and  
D. Archer

Title Page

Abstract

Introduction

Conclusions

References

Tables

Figures

⏪

⏩

◀

▶

Back

Close

Full Screen / Esc

Printer-friendly Version

Interactive Discussion



If  $r < R_{\text{break}}$ , the particle fragments into a number of daughter particles. From Goldthwait et al. (2004) we construct a power law with support between 2 and 24 integers (fragments) that describes the number of fragments,  $f$ , a particle breaks into:

$$P_f = \sum_{i=2}^f 0.91 \cdot i^{-1.56}. \quad (32)$$

- 5 A random number,  $r$ , is compared to  $P_f$  for each successive number of fragments starting from 2. When  $r < P_f$ , the number of fragments the aggregate breaks into is found. It is unlikely that very small particles will be fragmented because of how  $R_{\text{break}}$  is constructed, however, if  $f > p$ , then we let  $f = p$  meaning the particle fragments into its primary particles. Mass is always conserved during coagulation or fragmentation.
- 10 When a particle is fragmented,  $p_{\text{new}} = p_{\text{old}}/f$  and  $n_{\text{new}} = n_{\text{old}} \cdot f$ , here  $p_{\text{new}}$ ,  $n_{\text{new}}$ ,  $p_{\text{old}}$  and  $n_{\text{old}}$  stand for  $p$  and  $n$  after and before fragmentation respectively. If  $p_{\text{old}}$  can not be divided into an integer for the given number of fragments, it is divided into the nearest integer below and the remainder mass is divided between the particles and added without adding primary particles. For example, if  $p_{\text{old}} = 17$ ,  $n_{\text{old}} = 1$  and  $f = 3$ , then
- 15  $p_{\text{new}} = 5$ ,  $n_{\text{new}} = 3$  and the mass of 2 primary particles is divided between the 3 new aggregates. Here we compromise in conserving the number of primary particles but do conserve mass.

## 2.7.2 Ingestion

- If the particle is fragmented, it cannot be ingested in the same time step, but if it is not fragmented, then it is evaluated for ingestion. To prevent zooplankton from ingesting mineral particles with no orgC and dissolving and repackaging those minerals, an ad-hoc parameter is introduced which adjusts the probability of ingestion as a function of orgC concentration. The orgC weight fraction,  $\text{orgC}_{\text{wf}}$ , is calculated and compared to a random number  $r$ . If  $r < \text{orgC}_{\text{wf}}$ , the particle is deemed appetitive and ingested.
- 25 The model is sensitive to the choice of this parameter. If we choose  $r < 10\text{orgC}_{\text{wf}}$  or

## Sinking aggregates

T. Jokulsdottir and  
D. Archer

Title Page

Abstract

Introduction

Conclusions

References

Tables

Figures

◀

▶

◀

▶

Back

Close

Full Screen / Esc

Printer-friendly Version

Interactive Discussion



$r < 0.1 \text{orgC}_{\text{wf}}$  that decreases the orgC flux by half and increases the orgC flux 3–5 fold, respectively.

### 2.7.3 OrgC assimilation

The fraction of primary production grazed by microzooplankton estimated using dilution techniques (Landry and Hassett, 1982), leads to 60–75 % of primary production is consumed by protists and between 2–10 % is consumed by macro-grazers (Landry and Calbet, 2004). Other studies find that the fraction of production consumed by protists is perhaps a little lower, between 20 and 70 % (Kiorboe, 2000), 22–44 % (Riser et al., 2008), and 40–60 % (Richardson et al., 2004). The relative rates of carbon consumption in the deep ocean between bacteria and zooplankton vary regionally for reasons that are not well understood (Steinberg et al., 2008; Robinson et al., 2010). By satisfying that about 60–90 % of orgC that is ingested by zooplankton is assimilated and the remaining 10–40 % is egested in fecal pellets (Tande and Slagstad, 1985; Dilling et al., 1998; Bochdansky et al., 1999) we come up with this equation for zooplankton assimilation:

$$d \text{orgC}_i = 0.9 \cdot \left(1 - 2^{i-11}\right) \exp(\ln 2(T - 30)/10). \quad (33)$$

Since  $R_{\text{enc}}$  contains a timestep term, this assimilation term does not contain  $dt$ . In the model, fecal pellets are represented similarly to aggregates, with the difference that their porosity is specified to be 50 %, determined by the constraint of the settling velocity of model fecal pellets as a function of fecal pellet volume found by Small et al. (1979) (Sect. 2.4).

### 2.7.4 Biogenic mineral dissolution

pH of the guts of zooplankton increases during feeding, most likely due to dissolution of calcium carbonate (Pond et al., 1995). Jansen and Wolf-Gladrow (2001) model zooplankton gut chemistry and conclude that up to 10 % of ingested calcium carbonate

## Sinking aggregates

T. Jokulsdottir and  
D. Archer

Title Page

Abstract

Introduction

Conclusions

References

Tables

Figures

◀

▶

◀

▶

Back

Close

Full Screen / Esc

Printer-friendly Version

Interactive Discussion



## Sinking aggregates

T. Jokulsdottir and  
D. Archer

Title Page

Abstract

Introduction

Conclusions

References

Tables

Figures

I◀

▶I

◀

▶

Back

Close

Full Screen / Esc

Printer-friendly Version

Interactive Discussion



can be dissolved during the passage through the gut. Zooplankton mediated  $\text{CaCO}_3$  dissolution may help explain the apparent 60–80 % decrease in  $\text{CaCO}_3$  sinking flux in the upper 500–1000 m of the water column (Milliman et al., 1999), and the water column alkalinity source detected by Feely et al. (2004). In SLAMS, dissolution of  $\text{CaCO}_3$  in zooplankton guts is related to the fraction of the orgC that is assimilated:

$$d\text{CaCO}_3(i) = kZ_{\text{CaCO}_3(i)} \frac{d\text{orgC}}{\text{orgC}} \text{CaCO}_3(i) dt. \quad (34)$$

Where  $\text{CaCO}_3(1)$  stands for calcite,  $\text{CaCO}_3(2)$  represents aragonite and  $kZ_{\text{CaCO}_3(i)}$  is  $2 \times 10^{-2} \text{ s}^{-1}$  for calcite and  $4 \times 10^{-3} \text{ s}^{-1}$  for aragonite.

## 2.8 Abiotic mineral dissolution

In addition to biological dissolution of  $\text{CaCO}_3$  in zooplankton guts, there appears to be significant dissolution of the more soluble  $\text{CaCO}_3$  mineral aragonite in the water column (Gangsto et al., 2008). A significant fraction of the  $\text{CaCO}_3$  production flux is composed of aragonite (Fabry and Deuser, 1991), produced for example by pteropods. Water column conditions reach undersaturation with respect to aragonite at a shallower water depth than for calcite. Biogenic silica (bSi), the other main biomineral in the ocean, is undersaturated throughout the ocean, and is distinguished by a strong temperature sensitivity of its dissolution rate, dissolving significantly faster in warm waters (Gnanadesikan, 1999). In the deep ocean, carbonate dissolution is a function of the degree of undersaturation:

$$d\text{CaCO}_3(i) = kt_{\text{CaCO}_3(i)} \cdot \Omega \cdot \text{CaCO}_3(i) dt \quad (35)$$

where

$$\Omega = (1 - [\text{CO}_3^{=}]_{\text{in situ}} / [\text{CO}_3^{=}]_{\text{sat}})^n \quad (36)$$

is the saturation state of the sea water for calcite and aragonite.  $kt(1) = 5$ ,  $kt(2) = 3.2 \text{ day}^{-1}$ ,  $\eta = 4.5$  for calcite and 4.2 for aragonite. The carbonate ion profile or concentration with depth,  $[\text{CO}_3^{2-}]_{\text{in situ}}$ , is prescribed and dissolution of calcium carbonate does not feed back on it.

5 For bSi dissolution, the dissolution rate is calculated as

$$db\text{Si} = k_{\text{size}} \cdot R_d(T) \cdot b\text{Si} dt \quad (37)$$

with temperature sensitivity from Gnanadesikan (1999) as

$$R_d(T) = 1.32 \times 10^{16} \exp(-11481/T) \quad (38)$$

and a size-dependent term

$$10 \quad k_{\text{size}} = \frac{b\text{Si}}{b\text{Si} + 1 \times 10^{-10}} \quad (39)$$

to simulate the protective organic matrix or membrane that coats live diatoms and serves as protection to dissolution of frustules (Lewin, 1961; Kamatani, 1982). We presume that non-aggregated diatom cells are alive and thus have a coating to protect them from dissolving. Figure 5 shows the sensitivity of organic carbon, biogenic silica, calcium carbonate and terrestrial material flux to changes in  $k_{\text{size}}$ . If diatoms in the model are allowed to readily dissolve ( $k_{\text{size}} = 1$ ), very little bSi makes it to the seafloor and the organic carbon flux is decreased by 50 %.

## 2.9 Photodissolution

20 Ascending aggregates that are in the 1 m surface layer and larger than 1 cm in radius are broken down by sunlight. In response to a film of TEP-rich particles occasionally accumulating at the sea surface of the model we looked for mechanisms that would be a sink for those aggregates. Sunlight breaks down organic matter. DOC is turned into smaller molecules (Kieber et al., 1989) and in the laboratory POC has been found

to turn to DOC (Mopper et al., 1991). In the model we construct photolysis such that if  $r_a > 1$  cm and the aggregate is in the top 1 m of the water column and  $\rho_a < \rho_{sw}$  the aggregate is removed and considered dissolved.

## 2.10 Sea surface temperature

5 The temperature profiles are a linear interpolation from the SST to 5 °C at 1 km to 2 °C at 4 km; they do not include an isothermal mixed layer. In the model, the temperature is constant over the course of the year.

## 2.11 Carbonate ion profile

10 The carbonate ion concentration is set to 220  $\mu\text{mol kg}^{-1}$  at the sea surface and 80  $\mu\text{mol kg}^{-1}$  below 1 km depth. It is linearly interpolated between the surface and 1 km.

## 2.12 Bloom index

15 The bloom index describes the degree to which production is characterized by blooms:  $\text{BI} = \text{productive days}/365$ , such that  $\text{BI} = 1$  represents constant production throughout the year and  $\text{BI} = 0.25$  means that the annual production all takes place in a quarter of a year.

## 2.13 A time step

20 In a time step (Fig. 4) a small number (default = 21) of new particles are produced near the sea surface and their attributes such as composition, sinking velocity and stickiness are set. The water column is divided into depth bins ( $dz = 10$  m). For pairs of ACs with in a particular depth range (bin), the probability of aggregation is calculated and compared to a random number to assess whether the pair should stick. If so, the attributes of both particles involved are updated, the more numerous class losing members to aggregation with the less numerous class, which aggregates entirely. The

## Sinking aggregates

T. Jokulsdottir and  
D. Archer

Title Page

Abstract

Introduction

Conclusions

References

Tables

Figures

◀

▶

◀

▶

Back

Close

Full Screen / Esc

Printer-friendly Version

Interactive Discussion



## Sinking aggregates

T. Jokulsdottir and  
D. Archer[Title Page](#)[Abstract](#)[Introduction](#)[Conclusions](#)[References](#)[Tables](#)[Figures](#)[I◀](#)[▶I](#)[◀](#)[▶](#)[Back](#)[Close](#)[Full Screen / Esc](#)[Printer-friendly Version](#)[Interactive Discussion](#)

encounter rate of each AC to zooplankton is also calculated for each depth bin. Next, the model loops through every AC and: checks if it encountered zooplankton, respire orgC and TEP, dissolves minerals, disintegrates if there is not enough TEP to hold it together, ages orgC and TEP, checks if the size is small and considered to be dissolved, destroys orgC by photolysis, calculates new sinking velocity and settles or ascends accordingly. When the AC reaches the seafloor, it's content is cleared and memory is freed for a new aggregate.

### 3 Model validation

#### 3.1 Model–model comparison

The most common approach to modeling the flux of material through the water column is using a spectrum of particle size classes that aggregate according to coagulation theory, based on the sectional method of Jackson (1990). In that model, a reasonable number of size bins (10 or 100) hold concentrations of particles and the transfer of material between size bins by aggregation and fragmentation is calculated using the Smoluchowski equation. It is able to reproduce the slope of the particle size spectrum (log of number spectrum plotted against log of the particle radius) typically found in marine environments (Jackson, 1990, 1995).

The rationale for using a Monte Carlo method over a deterministic method is the large number of chemical components that can be resolved while keeping the model numerically feasible. The runtime of a deterministic coagulation model with  $N$  chemical components is proportional to  $(a \cdot b)^N$  where  $a$  and  $b$  are the number of size bins and composition-ratio-bins. In contrast, for a stochastic model, the runtime of a stochastic aggregation simulation is proportional to the number of aggregate classes squared, and does not increase with  $N$ .

Variations of the Monte Carlo method for aggregation developed by Gillespie (1975) are used to study aggregation in astrophysics (Ormel and Spaans, 2008; Zsom and

## Sinking aggregates

T. Jokulsdottir and  
D. Archer

Title Page

Abstract

Introduction

Conclusions

References

Tables

Figures

I ◀

▶ I

◀

▶

Back

Close

Full Screen / Esc

Printer-friendly Version

Interactive Discussion



Dullemond, 2008; Shima et al., 2009), atmospheric chemistry (Rierner et al., 2009; Shima et al., 2009), and oceanography (Khelifa and Hill, 2006; El Saadi and Bah, 2007). The approaches vary to fit the goal of each study, for example, in whether mass or number of aggregate classes is conserved, and in how many true particles an aggregate class represents.

One computational difference between our model and some of these is that we use a super-droplet method (Shima et al., 2009; Ormel and Spaans, 2008; Zsom and Dullemond, 2008), where each simulated particle (aggregate class) represents a large and variable number of real particles. The super-droplet method bypasses computational problems that have historically been considered a great drawback of Monte Carlo methods. Another distinction is that our model allows multi-stage aggregation within a given time step.

Many published plankton aggregation models differ from ours in scope, in that we track the particles not just through aggregation and export from the surface ocean, but throughout the water column to capture the entire biological pump. Other model treatments of the mechanics of the biological pump through the water column (Kriest and Evans, 2000; Stemmann et al., 2004) have been sectional formulation models.

To assess the validity of the aggregation method described above, we first look at the evolution of the particle spectrum with time where particles are not allowed to sink and the collision kernel is set to constant. We compare this spectrum to the analytical solution as presented by Wetherill (1990) (Fig. 6a). In the second test we allow the particles to sink and the curvilinear collision kernel used in SLAMS is used to determine aggregation. We look at the decrease of the mass remaining in the top box with time as also studied by Burd and Jackson (1997) (Fig. 6b).

The Monte Carlo algorithm is able to reproduce the time evolution of the particle size spectrum when a minimum of 100 computational particles are tracked. (For the full model runs described below, the number of computational particles reached about 30 000.) As the statistical significance of the larger particle size class in the Monte

Carlo model declines, its abundance is subject to random fluctuations, as seen in the large variations in the Monte Carlo model at  $t = 64$  (Fig. 6a).

### 3.2 Model-data comparison

Particle size distribution is a property of marine system; it provides information about the structure of the ecosystem and particle dynamics. The particle size spectrum in the ocean has been measured using particle counters and imaging methods. The slope of the particle size spectrum is usually calculated by dividing the concentration  $\Delta C$  of particles in a given size range  $\Delta r$  by the size range:  $n = \Delta C / \Delta r$ . In the ocean, the slope of the particle spectrum is found to be in the range  $-2$  to  $-5$  and in the model it is mostly around  $-3$ . In the model, the slope is steeper in the upper water column than in the deeper ocean, especially at the smaller end of the spectrum (Fig. 7). In contrast to the particle spectrum slope in the real ocean, the slope in SLAMS does not vary dramatically with changes in temperature, functional groups or primary production. That is perhaps a result of the simplistic representation of zooplankton ecology currently resolved.

To see how well the model captures the flux of material in the water column we compare three model results to data: the orgC flux in the water column, the pe-ratio and the rain ratio at the sea floor. Sediment trap data exist in a low resolution, temporally and spatially. Existing data has been analyzed quite extensively (Lutz et al., 2002; Dunne et al., 2005; Honjo et al., 2008). Our comparison of data with the model is based on the synthesis of Lutz et al. (2002), who looked for correlations between surface conditions and the magnitude and Martin depth scale of trap fluxes from 11 different regions of the world ocean. Table 2 shows the values of model driving parameters for the 11 regions and Fig. 8 compares model results with data. Except for the Panama Basin and the coast of NW Africa, the model predicts the flux to the seafloor within a factor of 2–5 (Fig. 8). The topography of the Panama Basin is complex and lateral transport of re-suspended material has been observed possibly explaining the high orgC flux seen in sediment traps Bishop et al. (1986). The North West African site is also unique; it has

## Sinking aggregates

T. Jokulsdottir and  
D. Archer

Title Page

Abstract

Introduction

Conclusions

References

Tables

Figures



Back

Close

Full Screen / Esc

Printer-friendly Version

Interactive Discussion



## Sinking aggregates

T. Jokulsdottir and  
D. Archer

Title Page

Abstract

Introduction

Conclusions

References

Tables

Figures

I◀

▶I

◀

▶

Back

Close

Full Screen / Esc

Printer-friendly Version

Interactive Discussion



a much higher primary productivity than other sites and the model overshoots predicting the orgC flux. In SLAMS, export is defined as flux out of the top 100 m as we do not model light attenuation or mixing. To see if the model captures relationships to do with export seen in the real world, model responses to sea surface temperature and rate of primary production are compared with data in Fig. 9. This data was compiled from field observations of primary production and particle export in Dunne et al. (2005). SLAMS produces the relationship between SST and export production quite well (Fig. 9a). The positive relationship seen in the data between export production and high PP is also produced by the model but because in most of our test cases PP is relatively low, this relationship is not demonstrated very clearly in Fig. 9d. No relationship is seen in the data between export production and SST, as well as between pe-ratio and PP. The model also sees no relationships between these pairs (Fig. 9b and c respectively).

Lastly, we compare the rain ratio (organic: inorgC) in the sinking carbon flux at the seafloor with rain ratio data (Honjo et al., 2008). SLAMS reproduces the observed value of approximately 1 in the tropics with higher values in the subtropics and polar latitudes (Fig. 10). The organic: inorgC ratio of primary production is the same in all model runs except for the Southern Ocean, run where biS production is doubled but CaCO<sub>3</sub> production is halved.

#### 4 What controls variability in the flux of orgC?

We assess the response of the model to three environmental parameters: the temperature profile, rate of primary production, and the bloom index. Figure 12 shows the fraction of primary production that sinks from the euphotic zone (the pe-ratio) and reaches the seafloor (the seafloor ratio) as a function of these parameters. The model responds the strongest to SSTs. An increase of 1° results in approximately 1.5% decrease in the pe-ratio (Fig. 12). For the default setting (SST = 20 C, PP = 1000 mg C m<sup>-2</sup> day, BI = 1) most of the flux is via particles with  $r < 1$  mm and  $v < 100$  m d<sup>-1</sup>. For lower SSTs, the orgC flux increases for all particle sizes. Remineralization rates increase with temper-

## Sinking aggregates

T. Jokulsdottir and  
D. Archer

Title Page

Abstract

Introduction

Conclusions

References

Tables

Figures



Back

Close

Full Screen / Esc

Printer-friendly Version

Interactive Discussion



ature, resulting in fewer particles that transport less orgC. Curiously, although larger particles are produced in a watercolumn with lower SST, those large particles don't contribute a large fraction of the flux (Fig. 11a and b). The sea floor is also sensitive to changes in SST: as sea surface temperatures drop more orgC makes it to the sea floor. It is most sensitive at low SSTs. Given other things are equal, a lower SST increases the efficiency of the biological pump.

An increase in primary production increases the number density of particles and the rate of aggregation. More large particles are produced that have high sinking velocity where PP is high (Fig. 11c and d). OrgC is exported and transported to the seafloor more efficiently where PP is high (Fig. 12c and d). The pe-ratio is more sensitive to changes in PP where PP is low. This effect is more pronounced in cool SSTs. For example, comparing PP at 1400 with 2000 (43% increase in PP) results in a 100% increase in orgC flux to the sea floor, primarily contributed by particles at the large end of the spectrum (Fig. 11c and d). The effect on the size spectrum when PP increases differs from the effect when SST is decreased. Contrary to when SST was decreased, large particles play a more pronounced role when PP is increased and contribute more to the increased flux than small particles (Fig. 11).

Both the pe-ratio and the seafloor ratio are sensitive to the bloom index. Blooms transport orgC more efficiently to depths. Organic carbon flux to the seafloor is approximately doubled when annual production takes place in a third of a year compared to when it is spread evenly throughout the year. The effect of concentrating production in blooms is the same as increasing PP; an increase in cell number densities enhances aggregation and produces more large and rapidly sinking aggregates (Fig. 11e and f).

Our results suggest that the biological pump is most efficient in environments that have low SSTs and high or sporadic primary production, such as polar environments. Our model shows the biological pump is also most sensitive in polar conditions. For example, in a global warming scenario where an increase in stratification leads to a smaller nutrient supply to the surface and a decrease in PP, it predicts greater organic carbon transport decrease in a polar environment than in a tropical environment.

Similarly, a 2° increase in SST would result in a greater decrease of orgC transport in a polar environment than in a tropical environment.

## 5 Conclusions

We present a new computational approach to simulating the biological pump from the surface ocean to the deep sea by resolving collections of individual particles. The method allows the model to resolve detailed attributes of the particles that may affect their sinking/degradation dynamics, including the mineral fraction, the age distribution of the organic matter, and the impact of transparent exopolymer particles (TEP) on particle aggregation. The model is able to reproduce sinking fluxes of orgC through the water column observed in sediment traps, and some of its regional variation. The model fluxes are sensitive to the three driving parameters analyzed: SST, primary production, and bloom index. The mechanistic links between these climate-sensitive drivers and the physics and chemistry of sinking particles in the ocean will enable us to predict the direction and magnitude of an ocean biological pump carbon cycle feedback to climate change, both in the past and in the future.

### Code availability

The code is available at github: <https://github.com/tinnsi/SLAMS>.

**The Supplement related to this article is available online at [doi:10.5194/gmdd-8-5931-2015-supplement](https://doi.org/10.5194/gmdd-8-5931-2015-supplement).**

*Acknowledgements.* We thank Oli Atlason for consulting on probability and statistics and Fred Ciesla and Adrian Burd for helpful discussion on coagulation. This work was supported by Grant OCE0628629 from NSF.

## Sinking aggregates

T. Jokulsdottir and  
D. Archer

Title Page

Abstract

Introduction

Conclusions

References

Tables

Figures

◀

▶

◀

▶

Back

Close

Full Screen / Esc

Printer-friendly Version

Interactive Discussion



## References

- Allredge, A. and Gotschalk, C.: In situ settling behavior of marine snow, *Limnol. Oceanogr.*, 33, 339–351, 1988. 5933, 5944
- Allredge, A. and McGillivray, P.: The attachment probabilities of marine snow and their implications for particle coagulation in the ocean, *Deep-Sea Res.*, 38, 431–443, 1991. 5936
- Allredge, A. and Silver, M. W.: Characteristics, dynamics and significance of marine snow, *Prog. Oceanogr.*, 20, 41–82, 1988. 5942
- Allredge, A., Granata, G. C., Gotschalk, C. C., and Dickey, T. D.: The physical strength of marine snow and its implications for particle disaggregation in the ocean, *Limnol. Oceanogr.*, 35, 1415–1428, 1990. 5934, 5946, 5947
- Allredge, A., Gotschalk, C., Passow, U., and Riebesell, U.: Mass aggregation of diatom blooms: insights from a mesocosm study, *Deep-Sea Res. Pt. II*, 42, 9–27, 1995. 5937
- Alonso-Gonzalez, I., Aristegui, J., Lee, C., Sanchez-Vidal, A., Calafat, A., Fabres, J., Sangra, P., Masque, P., Hernandez-Guerra, A., and Benitez-Barrios, V.: Role of slowly settling particles in the ocean carbon cycle, *Geophys. Res. Lett.*, 37, L13608, doi:10.1029/2010GL043827, 2010. 5933, 5944
- Armstrong, A. A., Lee, C., Hedges, J. I., Honjo, S., and Wakeham, S. G.: A new, mechanistic model for organic carbon fluxes in the ocean based on the quantitative association of POC with ballast minerals, *Deep-Sea Res. Pt. II*, 49, 219–236, 2002. 5933
- Arrigo, K. R., van Dijken, G. L., and Bushinsky, S.: Primary production in the Southern Ocean, *J. Geophys. Res.*, 113, C08004, doi:10.1029/2007JC004551, 2008. 5969
- Barber, R. T., Sanderson, M. P., Lindley, S. T., Chai, F., Newton, J., Trees, C. C., Foley, D. G., and Chavez, F. P., Primary productivity and its regulation in the equatorial Pacific during and following the 1991–1992 El Nino, *Deep-Sea Res. Pt. II*, 43, 933–969, 1996. 5969
- Barber, R. T., Marra, J., Bidigare, R. C., Codispoti, L. A., Halpern, D., Johnson, Z., Latasa, M., Goericke, R., and Smith, S. L.: Primary productivity and its regulation in the Arabian Sea during 1995, *Deep-Sea Res. Pt. II*, 48, 1127–1172, 2001. 5969
- Behrenfeld, M. J. and Falkowski, P. G.: Photosynthetic rates derived from satellite-based chlorophyll concentration, *Limnol. Oceanogr.*, 42, 1–20, 1997. 5969
- Berelson, W. M.: Particle settling rates increase with depth in the ocean, *Deep-Sea Res. Pt. II*, 49, 237–251, 2002. 5933, 5943

## Sinking aggregates

T. Jokulsdottir and  
D. Archer

Title Page

Abstract

Introduction

Conclusions

References

Tables

Figures

◀

▶

◀

▶

Back

Close

Full Screen / Esc

Printer-friendly Version

Interactive Discussion



## Sinking aggregates

T. Jokulsdottir and  
D. Archer

Title Page

Abstract

Introduction

Conclusions

References

Tables

Figures

I ◀

▶ I

◀

▶

Back

Close

Full Screen / Esc

Printer-friendly Version

Interactive Discussion



- Biddanda, B. A. and Pomeroy, L. R.: Microbial aggregation and degradation of phytoplankton-derived detritus in seawater. I. Microbial succession, *Mar. Ecol.-Prog. Ser.*, 42, 79–88, 1988. 5933
- Bishop, J. K. B., Stephien, J. C., and Wiebe, P. H.: Particulate matter distributions, chemistry and flux in the Panama Basin: response to environmental forcing, *Prog. Oceanogr.*, 17, 1–59, 1986. 5955
- Bochdanky, A. B., Deibel, D., and Rivkin, R. B.: Absorption efficiencies and biochemical fractionation of assimilated compounds in the cold water appendicularian *Oikopleura vanhoefeni*, *Limnol. Oceanogr.*, 44, 415–424, 1999. 5949
- Boyd, P. W. and Harrison, P. J.: Phytoplankton dynamics in the NE subarctic Pacific, *Deep-Sea Res. Pt. II*, 46, 2405–2432, 1999. 5969
- Boyd, P. W. and Trull, T. W.: Understanding the export of biogenic particles in oceanic waters: Is there a consensus?, *Prog. Oceanogr.*, 46, 2405–2432, 2007. 5933
- Buesseler, K. O., Trull, T. W., Steinberg, D. K., Silver, M. W., Siegel, D. A., Saitoh, S.-I., Lam-borg, C. H., Lam, P. J., Karl, D. M., Jiao, N. Z., Honda, M. C., Elskens, M., Dehairs, F., Brown, S. L., Boyd, P. W., Bishop, J. K. B., and Bidgare, R. R.: VERTIGO (VERTical Transport In the Global Ocean): a study of particle sources and flux attenuation in the North Pacific, *Deep-Sea Res. Pt. II*, 55, 1522–1539, 2008. 5932
- Burd, A. and Jackson, G. A.: Predicting particle coagulation and sedimentation rates for a pulsed input, *J. Geophys. Res.*, 102, 10545–10561, 1997. 5937, 5938, 5954
- Burd, A. and Jackson, G. A.: Particle aggregation, *Annual Review of Marine Science*, 1, 65–90, 2009. 5937, 5938
- Chen, Y.-L. L.: Spatial and seasonal variations of nitrate-based new production and primary production in the South China Sea, *Deep-Sea Res. Pt. I*, 52, 319–340, 2005. 5969
- Dam, H. G. and Drapeau, D. T.: Coagulation efficiency, organic-matter glues and the dynamics of particles during a phytoplankton bloom in a mesocosm study, *Deep-Sea Res. Pt. II*, 42, 111–123, 1995. 5936
- Dilling, L. and Alldredge, A. L.: Fragmentation of marine snow by swimming macrozooplankton: a new process impacting carbon cycling in the sea, *Deep-Sea Res. Pt. I*, 47, 1227–1245, 1998. 5946
- Dilling, L., Wilson, J., Steinberg, D., and Alldredge, A. L.: Feeding by the euphausiid *Euphausia pacifica* and the copepod *Calanus pacificus* on marine snow, *Mar. Ecol.-Prog. Ser.*, 170, 189–201, 1998. 5949

## Sinking aggregates

T. Jokulsdottir and  
D. Archer

Title Page

Abstract

Introduction

Conclusions

References

Tables

Figures

I ◀

▶ I

◀

▶

Back

Close

Full Screen / Esc

Printer-friendly Version

Interactive Discussion



- Dorsey, N. E.: The Properties of Ordinary Water Substance, Reinhold Pub. Corp., New York, 1940. 5944
- Ducklow, H. W., Steinberg, D. K., and Buesseler, K. O.: Upper ocean carbon export and the biological pump, *Oceanography*, 14, 50–58, 2001. 5932
- 5 Dunne, J. P., Armstrong, R. A., Gnanadesikan, A., and Sarmiento, J. L.: Empirical and mechanistic models for the particle export ratio, *Global Biogeochem. Cy.*, 19, GB4026, doi:10.1029/2004GB002390, 2005. 5955, 5956
- El Saadi, N. and Bah, A.: An individual-based model for studying the aggregation behavior in phytoplankton, *Ecol. Model.*, 204, 193–212, 2007. 5954
- 10 Emerson, S. and Hedges, J. I.: Processes controlling the organic carbon content of open ocean sediments, *Paleoceanography*, 3, 621–634, 1988. 5933, 5945
- Engel, A.: The role of transparent exopolymer particles (TEP) in the increase in apparent particle stickiness ( $\alpha$ ) during the decline of a diatom bloom, *J. Plankton Res.*, 22, 485–497, 2000. 5936, 5937
- 15 Engel, A., Abramson, L., Szlosek, J., Liu, Z., Stewart, G., Hirschberg, D., Lee, C.: Investigating the effect of ballasting by  $\text{CaCO}_3$  in *Emiliania huxleyi*, II: decomposition of particulate organic matter, *Deep-Sea Res. Pt. II*, 56, 1408–1419, doi:10.1016/j.dsr2.2008.11.028, 2000. 5933
- Fabry, V. J. and Deuser, W. G.: Aragonite and magnesian calcite fluxes to the deep Sargasso Sea, *Deep-Sea Res.*, 38, 713–728, 1991. 5950
- 20 Feely, R. A., Nojiri, Y., Dickson, A., Sabine, C. L., Lamb, M. F., and Ono, T.: Impact of anthropogenic  $\text{CO}_2$  on the  $\text{CaCO}_3$  system in the oceans, *Science*, 305, 362–366, 2004. 5950
- Feinberg, L. R. and Dam, H. G.: Effects of diet on dimensions, density and sinking rates of fecal pellets of the copepod *Acartia tonsa*, *Mar. Ecol.-Prog. Ser.*, 175, 87–96, 1998. 5942
- Francois, R., Honjo, S., Krishfield, R., and Manganini, S.: Factors controlling the flux of organic carbon to the bathypelagic zone of the ocean, *Global Biogeochem. Cy.*, 16, 1087, doi:10.1029/2001GB001722, 2002. 5933
- 25 Friedlingstein, P., Bopp, L., Ciais, P., Dufresne, J.-L., Fairhead, L., and Orr, J.: Positive feedback between future climate change and the carbon cycle, *Geophys. Res. Lett.*, 28, 1543–1546, 2001. 5932
- 30 Gangstø, R., Gehlen, M., Schneider, B., Bopp, L., Aumont, O., and Joos, F.: Modeling the marine aragonite cycle: changes under rising carbon dioxide and its role in shallow water  $\text{CaCO}_3$  dissolution, *Biogeosciences*, 5, 1057–1072, doi:10.5194/bg-5-1057-2008, 2008. 5934, 5950

## Sinking aggregates

T. Jokulsdottir and  
D. Archer

Title Page

Abstract

Introduction

Conclusions

References

Tables

Figures

I ◀

▶ I

◀

▶

Back

Close

Full Screen / Esc

Printer-friendly Version

Interactive Discussion



- Gillespie, D.T.: An exact method for numerically simulating the stochastic coalescence process in a cloud, *J. Atmos. Sci.*, 32, 1977–1989, 1975. 5953
- Gnanadesikan, A.: A global model of silicon cycling: sensitivity to eddy parameterization and dissolution, *Global Biogeochem. Cy.*, 13, 199–220, 1999. 5934, 5950, 5951
- 5 Goldthwait, S., Yen, J., Brown, J., and Alldredge, A.: Quantification of marine snow fragmentation by swimming euphausiids, *Limnol. Oceanogr.*, 49, 940–952, 2004. 5948
- Graham, W. M., MacIntyre, S., and Alldredge, A. L.: Diel variations of marine snow concentration in surface waters and implications for particle flux in the sea, *Deep-Sea Res. Pt. I*, 47, 367–395, 2000. 5946
- 10 Grossart, H. P. and Ploug, H.: Bacterial production and growth efficiencies: direct measurements on riverine aggregates, *Limnol. Oceanogr.*, 45, 436–445, 2000. 5945
- Grossart, H. P. and Ploug, H.: Microbial degradation of organic carbon and nitrogen on diatom aggregates, *Limnol. Oceanogr.*, 46, 267–277, 2001. 5945, 5946
- Grossart, H. P., Hietanen, S., and Ploug, H.: Microbial dynamics on diatom aggregates in Ore-  
sund, Denmark, *Mar. Ecol.-Prog. Ser.*, 249, 69–78, 2003. 5945, 5946
- 15 Hedges, J. I. and Keil, R. G.: Sedimentary organic matter preservation: an assessment and speculative synthesis, *Mar. Chem.*, 49, 81–115, 1995. 5933
- Honjo, S., Manganini, S. J., Krishfield, R. A., and Francois, R.: Particulate organic carbon fluxes to the ocean interior and factors controlling the biological pump: a synthesis of global sediment trap programs since 1983, *Prog. Oceanogr.*, 76, 217–285, 2008. 5955, 5956, 5980
- 20 Huntsman, S. A. and Barber, R. T.: Primary production off northwest Africa: the relationship to wind and nutrient conditions, *Deep-Sea Res.*, 24, 25–33, 1977. 5969
- Jackson, G. A.: Model of the formation of marine algal flocs by physical coagulation processes, *Deep-Sea Res. Pt. I*, 37, 1197–1211, 1990. 5934, 5935, 5953
- 25 Jackson, G. A.: Comparing observed changes in particle size spectra with those predicted using coagulation theory, *Deep-Sea Res. Pt. II*, 42, 159–184, 1995. 5935, 5937, 5946, 5953
- Jansen, H. and Wolf-Gladrow, D. A.: Carbonate dissolution in copepod guts: a numerical model, comparing observed changes in particle size spectra with those predicted using coagulation theory, *Mar. Ecol.-Prog. Ser.*, 221, 199–207, 2001. 5949
- 30 Kahl, L. A., Vardi, A., and Schofield, O.: Effects of phytoplankton physiology on export flux, *Mar. Ecol.-Prog. Ser.*, 354, 3–19, 2008. 5936
- Kamatani, A.: Dissolution rates of silica from diatoms decomposing at various temperatures, *Mar. Biol.*, 68, 91–96, 1982. 5951

## Sinking aggregates

T. Jokulsdottir and  
D. Archer

Title Page

Abstract

Introduction

Conclusions

References

Tables

Figures

I ◀

▶ I

◀

▶

Back

Close

Full Screen / Esc

Printer-friendly Version

Interactive Discussion



- Khelifa, A. and Hill, P. S.: Kinematic assessment of floc formation using a Monte Carlo model, *Journal of Hydraulic Research*, 44, 548–559, 2006. 5954
- Kieber, D. J., McDaniel, J., and Mopper, K.: Photochemical source of biological substrates in sea water: implications for carbon cycling, *Nature*, 341, 637–639, 1989. 5951
- 5 Kiorboe, T.: Colonization of marine snow aggregates by invertebrate zooplankton: abundance, scaling, and possible role, *Limnol. Oceanogr.*, 45, 479–484, 2000. 5949
- Klaas, C. and Archer, D. E.: Association of sinking organic matter with various types of mineral ballast in the deep sea: implications for the rain ratio, *Global Biogeochem. Cy.*, 16, 1116, doi:10.1029/2001GB001765, 2002. 5933
- 10 Krause, J. W., Nelson, D. M., and Brzezinski, M. A.: Biogenic silica production and the diatom contribution to primary production and nitrate uptake in the eastern equatorial Pacific Ocean, *Deep-Sea Res. Pt. II*, 58, 434–438, 2011. 5969
- Kriest, I. and Evans, G. T.: A vertically resolved model for phytoplankton aggregation, *P. Indian AS-Earth*, 109, 453–469, 2000. 5954
- 15 Kwon, E. Y., Primeau, F., and Sarmiento, J. L.: The impact of remineralization depth on the air-sea carbon balance, *Nat. Geosci.*, 2, 630–635, 2009. 5932
- Lampitt, R. S., Wishner, K. F., Turley, C. M., and Angel, M. V.: Marine snow studies in the Northeast Atlantic Ocean: distribution, composition and role as a food source for migrating plankton, *Mar. Biol.*, 116, 689–702, 1993. 5946
- 20 Lampitt, R. S., Salter, I., de Cuevas, B. A., Hartman, S., Larkin, K. E., and Pebody, C. A.: Long-term variability of downward particle flux in the deep northeast Atlantic: causes and trends, *Deep-Sea Res. Pt. II*, 57, 1346–1361, 2010. 5969
- Landry, M. R. and Calbet, A.: Microzooplankton production in the oceans, *ICES J. Mar. Sci.*, 61, 501–507, 2004. 5949
- 25 Landry, M. R. and Hassett, R. P.: Estimating the grazing impact of marine micro-zooplankton, *Mar. Biol.*, 67, 283–288, 1982. 5949
- Lewin, J. C.: The dissolution of silica from diatom walls, *Geochim. Cosmochim. Ac.*, 21, 182–198, 1961. 5951
- Li, X. Y. and Logan, B. E.: Size distributions and fractal properties of particles during a simulated phytoplankton bloom in a mesocosm, *Deep-Sea Res. Pt. II*, 42, 128–138, 1995. 5942
- 30 Logan, B. E. and Wilkinson, D. B.: Fractal geometry of marine snow and other biological aggregates, *Limnol. Oceanogr.*, 35, 130–136, 1990. 5941, 5942, 5943

## Sinking aggregates

T. Jokulsdottir and  
D. Archer

Title Page

Abstract

Introduction

Conclusions

References

Tables

Figures

I◀

▶I

◀

▶

Back

Close

Full Screen / Esc

Printer-friendly Version

Interactive Discussion



- Logan, B. E., Passow, U., Alldredge, A. L., Grossart, H.-P., and Simon, M.: Rapid formation and sedimentation of large aggregates is predictable from coagulation rates (half-lives) of transparent exopolymers particles (TEP), *Deep-Sea Res. Pt. II*, 42, 203–214, 1995. 5936
- Lutz, M. J., Dunbar, R. B., and Caldeira, K.: Regional variability in the vertical flux of particulate organic carbon in the ocean interior, *Global Biogeochem. Cy.*, 16, 1037, doi:10.1029/2000GB001383, 2002. 5955, 5978
- Mari, X.: Does ocean acidification induce an upward flux of marine aggregates?, *Biogeosciences*, 5, 1023–1031, doi:10.5194/bg-5-1023-2008, 2008. 5937
- Martin, J. H., Knauer, G. A., Karl, D. M., and Broenkow, W. W.: VERTEX: carbon cycling in the northeast Pacific, *Deep-Sea Res.*, 34, 267–285, 1987.
- McDonnell, A. M. P. and Buesseler, K. O.: Variability in the average sinking velocity of marine particles, *Limnol. Oceanogr.*, 55, 2085–2096, 2010. 5944
- Middelburg, J. J.: A simple rate model for organic matter decomposition in marine sediments, *Geochim. Cosmochim. Ac.*, 53, 1577–1581, 1989. 5946
- Milliman, J. D., Troy, P. J., Balch, W. M., Adams, A. K., Li, Y.-H., and Mackenzie, F. T.: Biologically mediated dissolution of calcium carbonate above the chemical lysocline?, *Deep-Sea Res. Pt. I*, 46, 1653–1669, 1999. 5950
- Le Moigne, F. A. C., Gallinari, M., Laurenceau, E., and De La Rocha, C. L.: Enhanced rates of particulate organic matter remineralization by microzooplankton are diminished by added ballast minerals, *Biogeosciences*, 10, 5755–5765, doi:10.5194/bg-10-5755-2013, 2013. 5933
- Mopper, K., Zhou, X., Kieber, R. J., Kieber, D. J., Sikorski, R. J., and Jones, R. D.: Photochemical degradation of dissolved organic carbon and its impact on the oceanic carbon cycle, *Nature*, 353, 60–62, 1991. 5945, 5952
- Murnane, R. J., Cochran, J. K., Buesseler, K. O., and Bacon, M. P.: Least-squares estimates of thorium, particle, and nutrient cycling rate constants from JGOFS North Atlantic Bloom Experiment, *Deep-Sea Res. Pt. I*, 43, 239–258, 1996.
- Ormel, C. W. and Spaans, M.: Monte Carlo simulation of particle interactions at high dynamic range: advancing beyond the Googol, *Astrophys. J.*, 684, 1291–1309, 2008. 5953, 5954
- Passow, U. and De La Rocha, C. L.: Accumulation of ballast on organic aggregates, *Global Biogeochem. Cy.*, 20, GB1013, doi:10.1029/2005GB002579, 2006. 5933, 5934

## Sinking aggregates

T. Jokulsdottir and  
D. Archer

Title Page

Abstract

Introduction

Conclusions

References

Tables

Figures

I◀

▶I

◀

▶

Back

Close

Full Screen / Esc

Printer-friendly Version

Interactive Discussion



- Ploug, H. and Grossart, H.-P.: Bacterial growth and grazing on diatom aggregates: respiratory carbon turnover as a function of aggregate size and sinking velocity, *Limnol. Oceanogr.*, 45, 1467–1475, 2000. 5945, 5946
- Ploug, H., Iversen, M. H., and Fischer, G.: Ballast, sinking velocity, and apparent diffusivity within marine snow and zooplankton fecal pellets: implications for substrate turnover by attached bacteria, *Limnol. Oceanogr.*, 53, 1878–1886, 2008. 5933, 5942
- Pond, D. W., Harris, R. P., Brownlee, C.: A microinjection technique using a pH sensitive dye to determine the gut pH of calanus-helgolandicus, *Mar. Biol.*, 123, 75–79, 1995. 5949
- Richardson, K., Markager, S., Buch, E., Lassen, M. F., and Kristensen, A. S.: Seasonal distribution of primary production, phytoplankton biomass and size distribution in the Greenland Sea, *Deep-Sea Res. Pt. I*, 52, 979–999, 2005. 5969
- Richardson, T. L., Jackson, G. A., Ducklow, H. W., and Roman, M. R.: Carbon fluxes through food webs of the eastern equatorial Pacific: an inverse approach, *Deep-Sea Res. Pt. I*, 51, 1245–1274, 2004. 5949
- Riemer, N., West, M., Zaveri, R. A., and Easter, R. C.: Simulating the evolution of soot mixing state with a particle-resolved aerosol model, *J. Geophys. Res.*, 114, D09202, doi:10.1029/2008JD011073, 2009. 5954
- Riley, J. S., Sanders, R., Marsay, C., Le Moigne, F. A. C., Achterberg, E. P., and Poulton, A. J.: The relative contribution of fast and slow sinking particles to ocean carbon export, *Global Biogeochem. Cy.*, 26, GB1026, doi:10.1029/2011GB004085, 2012. 5933
- Riser, C. W., Wassmann, P., Reigstad, M., and Seuthe, L.: Vertical flux regulation by zooplankton in the northern Barents Sea during Arctic spring, *Deep-Sea Res. Pt. II*, 55, 2320–2329, 2008. 5949
- Robinson, C., Steinberg, D. K., Anderson, T. R., Aristegui, J., Carlson, C. A., Frost, J. R., Ghiglione, J.-F., Hernandez-Leon, S., Jackson, G. A., Koppelman, R., Queguiner, B., Ragneau, O., Rassoulzadegan, F., Robinson, B. H., Tamburini, C., Tanaka, T., Wishner, K. F., and Zhang, J.: Mesopelagic zone ecology and biogeochemistry – a synthesis, *Deep-Sea Res. Pt. II*, 57, 1504–1518, 2010. 5949
- Ruiz, J.: What generates daily cycles of marine snow?, *Deep-Sea Res. Pt. I*, 44, 1105–1126, 1997. 5946
- Saba, V. S., Friedrichs, M. A. M., Carr, M. E., Antoine, D., Armstrong, R. A., Asanuma, I., Aumont, O., Bates, N. R., Behrenfeld, M. J., Bennington, V., Bopp, L., Bruggeman, J., Erik, Buitenhuis, T., Church, M. J., Ciotti, A. M., Doney, S. C., Dowell, M., Dunne, J., Dutkiewicz, S.,

## Sinking aggregates

T. Jokulsdottir and  
D. Archer

Title Page

Abstract

Introduction

Conclusions

References

Tables

Figures

I ◀

▶ I

◀

▶

Back

Close

Full Screen / Esc

Printer-friendly Version

Interactive Discussion



Gregg, W., Hoepffner, N., Hyde, K. J. W., Ishizaka, J., Kameda, T., Karl, D. M., Lima, I., Lomas, M. W., Marra, J., McKinley, G. A., Melin, F., Moore, J. K., Morel, A., O'Reilly, J., Salihoglu, B., Scardi, M., Smyth, T. J., Tang, S., Tjiputra, J., Uitz, J., Vichi, M., Waters, K., Westberry, T. K., and Yool, A.: Challenges of modeling depth integrated marine primary productivity over multiple decades: a case study at BATS and HOT, *Global Biogeochem. Cy.*, 24, GB3020, doi:10.1029/2009GB003655, 2010. 5969

Schneider, B., Bopp, L., and Gehlen, M.: Assessing the sensitivity of modeled air-sea CO<sub>2</sub> exchange to the remineralization depth of particulate organic and inorganic carbon, *Global Biogeochem. Cy.*, 22, GB3021, doi:10.1029/2007GB003100, 2008. 5932

Shima, S., Kusano, K., Kawano, A., Sugiyama, T., and Kawahara, S.: The super-droplet method for the numerical simulation of clouds and precipitation: a particle-based and probabilistic microphysics model coupled with a non-hydrostatic model, *Q. J. Roy. Meteor. Soc.*, 135, 1307–1320, 2009. 5954

Small, L. F., Fowler, S. W., and Unlu, M. Y.: Sinking rates of natural copepod fecal pellets, *Mar. Biol.*, 51, 233–241, 1979. 5942, 5949

Steinberg, D. K., Van Mooy, B. A. S., Buesseler, K. O., Boyd, P. W., Kobari, T., and Karl, D. M.: Bacterial vs. zooplankton control of sinking particle flux in the ocean's twilight zone, *Limnol. Oceanogr.*, 53, 1327–1338, 2008. 5949

Stemann, L., Picheral, M., and Gorsky, G.: Diel variation in the vertical distribution of particulate matter (> 0.15 mm) in the NW Mediterranean Sea investigated with the Underwater Video Profiler, *Deep-Sea Res. Pt. I*, 47, 505–531, 2000. 5946

Stemann, L., Jackson, G. A., and Ianson, D.: A vertical model of particle size distributions and fluxes in the midwater column that includes biological and physical processes – Part I: model formulation, *Deep-Sea Res. Pt. I*, 51, 865–884, 2004. 5954

Tande, K. S. and Slagstad, D.: Assimilation efficiency in herbivorous aquatic organisms – the potential of the ratio method using I4C and biogenic silica as markers, *Limnol. Oceanogr.*, 30, 1093–1099, 1985. 5949

Trull, T. W., Bray, S. G., Buesseler, K. O., Lamborg, C. H., Manganini, S., Moy, C., and Valdes, J.: In situ measurements of mesopelagic particle sinking rates and the control of carbon transfer to the ocean interior during the Vertical Flux in the Global Ocean (VERTIGO) voyages in the North Pacific, *Geophys. Res. Lett.*, 55, 1684–1695, doi:10.1016/j.dsr2.2008.04.021, 2008. 5943

## Sinking aggregates

T. Jokulsdottir and  
D. Archer[Title Page](#)[Abstract](#)[Introduction](#)[Conclusions](#)[References](#)[Tables](#)[Figures](#)[I◀](#)[▶I](#)[◀](#)[▶](#)[Back](#)[Close](#)[Full Screen / Esc](#)[Printer-friendly Version](#)[Interactive Discussion](#)

Verdugo, P., Alldredge, A. L., Azam, F., Kirchman, D. L., Passowa, U., and Santschi, P. H.:  
The oceanic gel phase: a bridge in the DOM-POM continuum, *Mar. Chem.*, 92, 67–85,  
doi:10.1016/j.marchem.2004.06.017, 2004. 5936, 5937

Westrich, J. T. and Berner, R. A.: The role of sedimentary organic matter in bacterial sulfate  
reduction: the G model tested, *Limnol. Oceanogr.*, 29, 236–249, 1984. 5945

Wetherill, G. W.: Comparison of analytical and physical modeling of planetesimal accumulation,  
*Icarus*, 88, 336–354, 1990. 5954, 5976

White, F. M.: *Viscous Fluid Flow*, McGraw-Hill, 1991. 5944

Zsom, A. and Dullemond, C. P.: A representative particle approach to coagulation and  
fragmentation of dust aggregates and fluid droplets, *Astron. Astrophys.*, 489, 931–941,  
doi:10.1051/0004-6361:200809921 2008. 5953, 5954

## Sinking aggregates

T. Jokulsdottir and  
D. Archer

**Table 1.** Attributes of a particle that the computational particle keeps track of.

Attribute	Symbol	Units	Notes and equations
Identification number	id		used when listing particles according to depth
Water column or bottom	<i>b</i>		boolean variable to distinguish between particle in the water column and at sea floor
Aggregate or fecal pellet	af		boolean variable to distinguish between aggregate and fecal pellet
Scaling factor	<i>n</i>		number of real aggregates represented by the super aggregate
Primary particles	<i>p</i>		number of primary particles in a real particle
Primary particle radius	<i>r<sub>p</sub></i>	μm	$r_p = \sqrt[3]{\frac{3V_p}{4\pi}}, V_p = \frac{V_m}{\rho}, V_m = \sum_i X_i \frac{mw_i}{\rho_i}^*$
Fractal dimension	<i>D<sub>N</sub></i>		$D_N = 2$
Aggregate radius aggregate	<i>r<sub>a</sub></i>	μm	$r_a = r_p \cdot \rho^{1/D_N}$
Porosity	<i>φ</i>		$\phi = 1 - \rho \left(\frac{r_p}{r_a}\right)^3$
Density of aggregate	<i>ρ</i>	gcm <sup>-3</sup>	$\rho = \rho_s(1 - \phi) + \rho_{sw}\phi, \rho_s = \sum_i X_i mw_i / V_m^*$
Stickiness	<i>α</i>		$\alpha = V_{TEP} / V_m^*$
Depth	<i>z</i>	m	
Sinking velocity	<i>u</i>	cms <sup>-1</sup>	$u = g(\rho - \rho_{sw})(2r_a)^2 / 18\rho_{sw}\nu$
Organic carbon	orgC(1...10)	mol C	10 types (ages) of organic carbon
Transparent exopolymer particles	TEP(1...10)	mol C	10 types (ages) of TEP
Minerals	mrl(1...4)	mol	calcite, aragonite, bSi and lithogenic material

\*  $i(1, \dots, 6) = \sum_{age=1}^{10} orgC_{age}, \sum_{age=1}^{10} TEP_{age}, calcite, aragonite, bSi, dust.$

Title Page

Abstract Introduction

Conclusions References

Tables Figures

◀ ▶

◀ ▶

Back Close

Full Screen / Esc

Printer-friendly Version

Interactive Discussion



## Sinking aggregates

T. Jokulsdottir and  
D. Archer**Table 2.** Environmental variables for the 11 regions. Primary production in [ $\text{mgC m}^{-2} \text{d}^{-1}$ ]. Reference for the primary production.

Region	SST [ $^{\circ}\text{C}$ ]	Prim. Prod.	BI	Reference
Greenland Norwegian Seas	3	240	0.5	Richardson et al. (2005)
North Atlantic (NABE)	14	500	0.75	Lampitt et al. (2010)
Sargasso Sea (BATS)	22	500	0	Saba et al. (2010)
Subarctic Pacific (OSP)	14	500	0.75	Boyd and Harrison (1999)
N. C. Pacific Gyre (HOT)	23	500	0	Saba et al. (2010)
Equatorial Pacific	24	1000	0	Barber (1996) and Krause et al. (2011)
South China Sea	24	500	0	Chen (2005)
Southern Ocean	3	200	0.5	Arrigo et al. (2008)
Arabian Sea	26	1000	0	Barber (2001)
Panama Basin	24	600	0	Behrenfeld and Falkowski (1997)
NW Africa	24	2000	0	Huntsman and Barber (1977)

Title Page

Abstract

Introduction

Conclusions

References

Tables

Figures

I ◀

▶ I

◀

▶

Back

Close

Full Screen / Esc

Printer-friendly Version

Interactive Discussion



## Sinking aggregates

T. Jokulsdottir and  
D. Archer

**Table 3.** The probability,  $P$ , for a type of particle to be produced and range of values compared to a random number to determine the type produced, the amount of material in each particle [ $\text{pmol particle}^{-1}$ ],  $n$  is the number of particles produced each time. Radius,  $r$  [ $\mu\text{m}$ ], density,  $\rho$  [ $\text{gcm}^{-3}$ ]. (Particle types: C = coccolithophorid, A = Aragonite forming phytoplankton, D = diatom, Pi = picoplankton, D = dust.)

Type	$P$	Range	orgC	calcite	arag.	bSi	clay	$n$	$r$	$\rho$
C	0.04	0–0.04	7	1.5	0	0	0	$1.98 \times 10^8$	3.9	1.92
A	0.02	0.04–0.06	7	0	1.5	0	0	$1.98 \times 10^8$	3.9	1.92
D	0.24	0.06–0.30	15	0	0	5	0	$9.26 \times 10^7$	5.3	1.24
Pi	0.69	0.3–0.99	1	0	0	0	0	$1.39 \times 10^9$	1.9	1.06
D	0.01	0.99–1	0	0	0	0	2.85	$4.88 \times 10^8$	1.15	2.65

Title Page

Abstract

Introduction

Conclusions

References

Tables

Figures

I ◀

▶ I

◀

▶

Back

Close

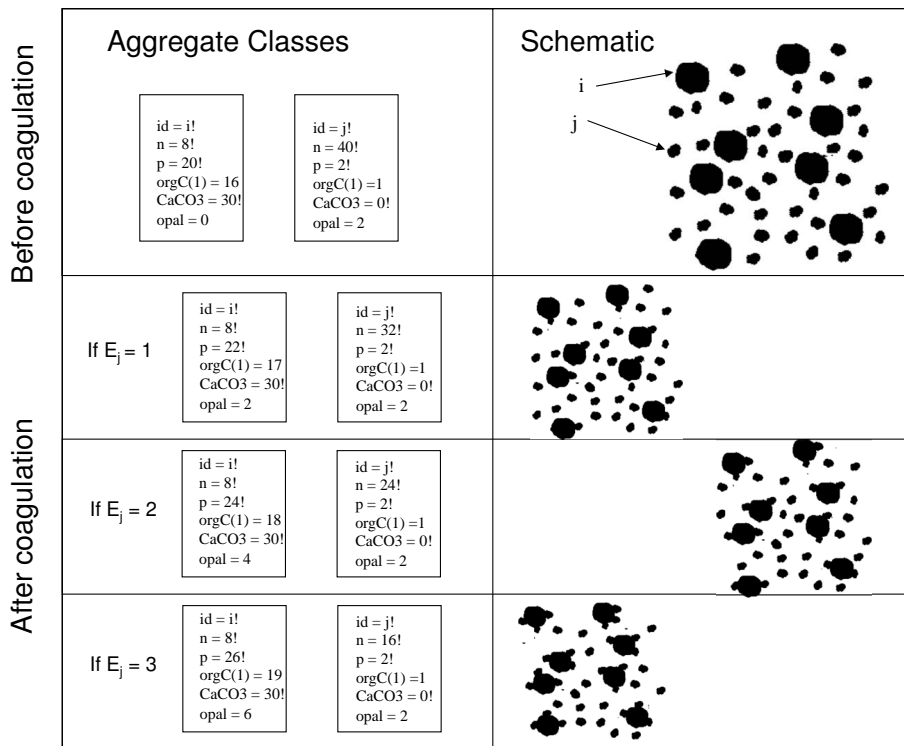
Full Screen / Esc

Printer-friendly Version

Interactive Discussion

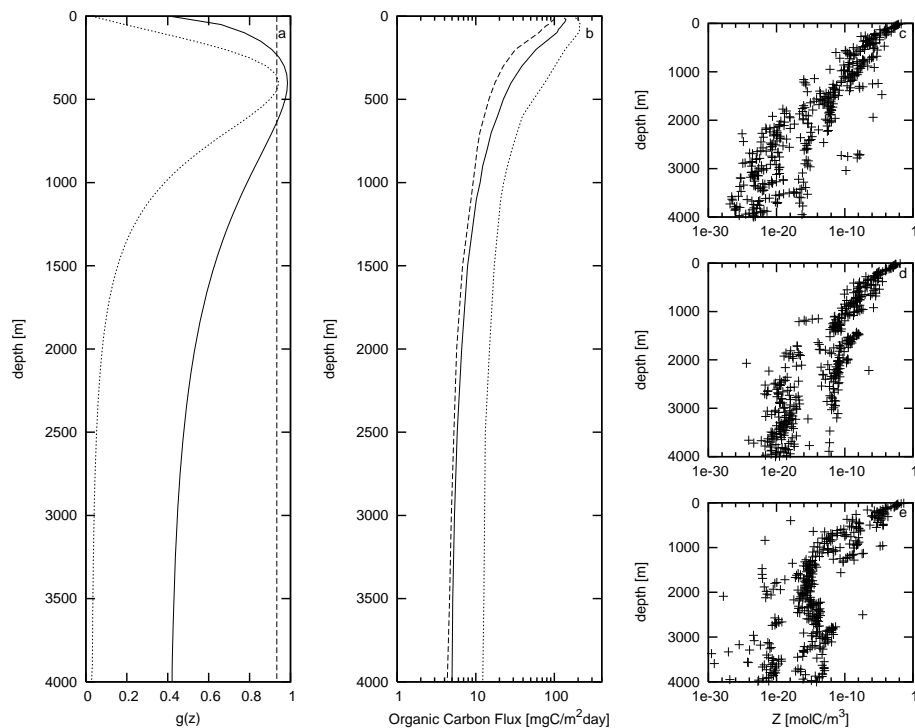






**Figure 2.** An example of two computational particles sticking. Top left shows super aggregates  $i$  and  $j$  before coagulation takes place. Top right a schematic of the aggregates the computational particles represent. Bottom three rows shows super aggregates if  $E_j = 1, 2$ , or  $3$ . Note that the total number of primary particles is conserved;  $n_i p_i + n_j p_j = 240$  before and after coagulation. Same is true for the amount of organic carbon,  $\text{CaCO}_3$  and bSi.

[Title Page](#)
[Abstract](#)
[Introduction](#)
[Conclusions](#)
[References](#)
[Tables](#)
[Figures](#)
[I ◀](#)
[▶ I](#)
[◀](#)
[▶](#)
[Back](#)
[Close](#)
[Full Screen / Esc](#)
[Printer-friendly Version](#)
[Interactive Discussion](#)

**Figure 3.** Metabolic efficiency scaling factor,  $g(z)$ , in SLAMS (solid line), a constant factor (dashed line) and a smaller factor (dotted line) **(a)**. The corresponding organic carbon flux **(b)**. Three plots on the left are corresponding amount of organic carbon in the water column,  $Z$ , for SLAMS **(c)**, constant factor **(d)** and smaller factor **(e)**.

## Sinking aggregates

T. Jokulsdottir and  
D. Archer

[Title Page](#)

[Abstract](#)

[Introduction](#)

[Conclusions](#)

[References](#)

[Tables](#)

[Figures](#)

[I◀](#)

[▶I](#)

[◀](#)

[▶](#)

[Back](#)

[Close](#)

[Full Screen / Esc](#)

[Printer-friendly Version](#)

[Interactive Discussion](#)

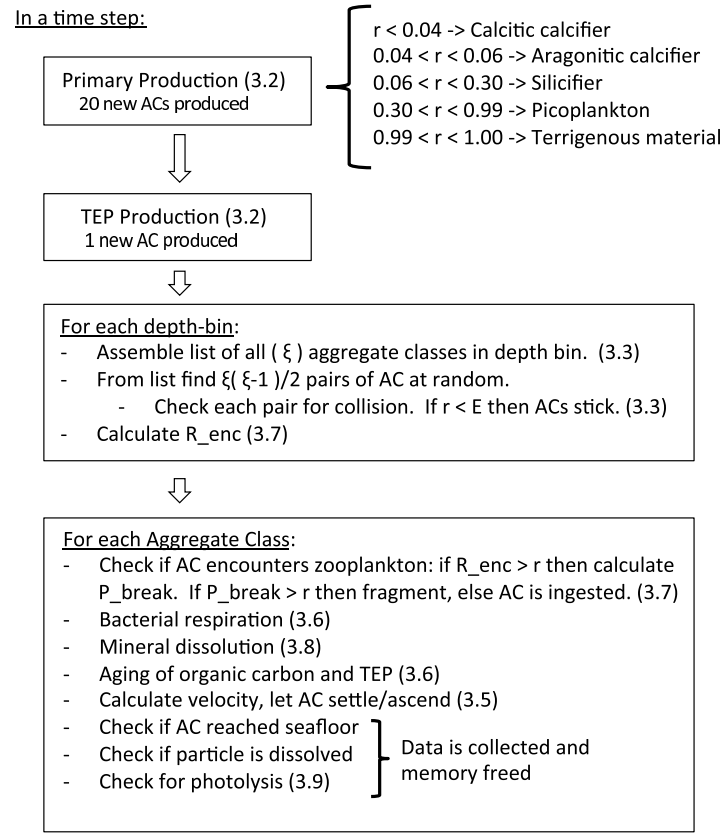


**Figure 4.** An outline of what the model does in a timestep. In parenthesis are the sections where each task is explained.

## Sinking aggregates

T. Jokulsdottir and  
D. Archer

Title Page

Abstract

Introduction

Conclusions

References

Tables

Figures

I ◀

▶ I

◀

▶

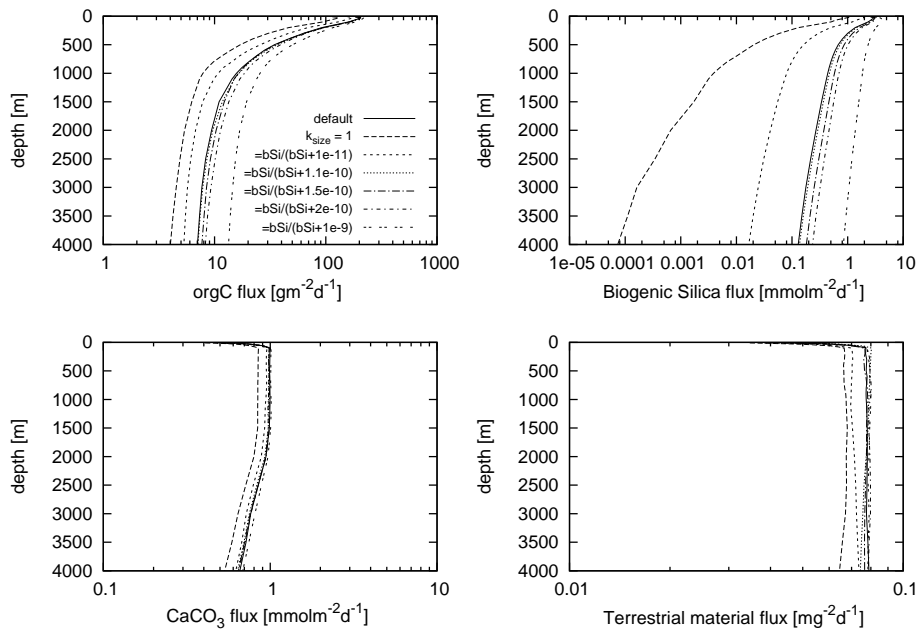
Back

Close

Full Screen / Esc

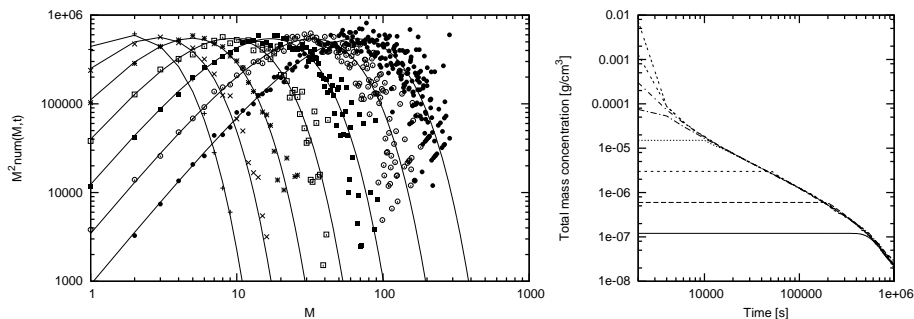
Printer-friendly Version

Interactive Discussion



**Figure 5.** Sensitivity of the flux to changes in  $k_{size}$ . Shown are 7 model runs changing  $k_{size}$  as depicted in the upper left panel.

## Sinking aggregates

T. Jokulsdottir and  
D. Archer

**Figure 6.** Analytical solution of the Smoluchovski equation Wetherill (1990) (solid lines) at times 1, 2, 4, . . . , 64 and model results for corresponding times: 1 (plus-signs), 2 (crosses), 4 (asterisk), 8 (open boxes), 16 (solid boxes), 32 (open circles), 64 (solid circles) **(a)**. 10 000 computational particles were used here and a total of  $1 \times 10^6$  particles. Results were averaged over 50 runs to generate this plot. For this comparison, particles do not sink and the collision kernel is a constant ( $1 \times 10^{-6}$ ). The vertical axis is the number of particles of mass  $M$  at time  $t$  times  $M^2$ . Variation of total mass with time **(b)** with the collision kernel used in SLAMS for 8 different initial concentrations. Particles coagulate and sink but are not altered by biological or chemical processes.

Title Page

Abstract

Introduction

Conclusions

References

Tables

Figures

◀

▶

◀

▶

Back

Close

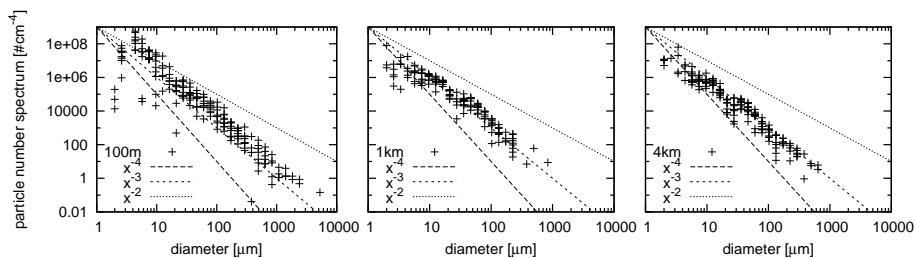
Full Screen / Esc

Printer-friendly Version

Interactive Discussion



## Sinking aggregates

T. Jokulsdottir and  
D. Archer

**Figure 7.** Particle number spectrum at three depths: 100 m, 1 and 4 km. In each panel, we plot the output for ten depth bins around the target depth.

[Title Page](#)[Abstract](#)[Introduction](#)[Conclusions](#)[References](#)[Tables](#)[Figures](#)[I◀](#)[▶I](#)[◀](#)[▶](#)[Back](#)[Close](#)[Full Screen / Esc](#)[Printer-friendly Version](#)[Interactive Discussion](#)

## Sinking aggregates

T. Jokulsdottir and  
D. Archer

Title Page

Abstract

Introduction

Conclusions

References

Tables

Figures

◀

▶

◀

▶

Back

Close

Full Screen / Esc

Printer-friendly Version

Interactive Discussion

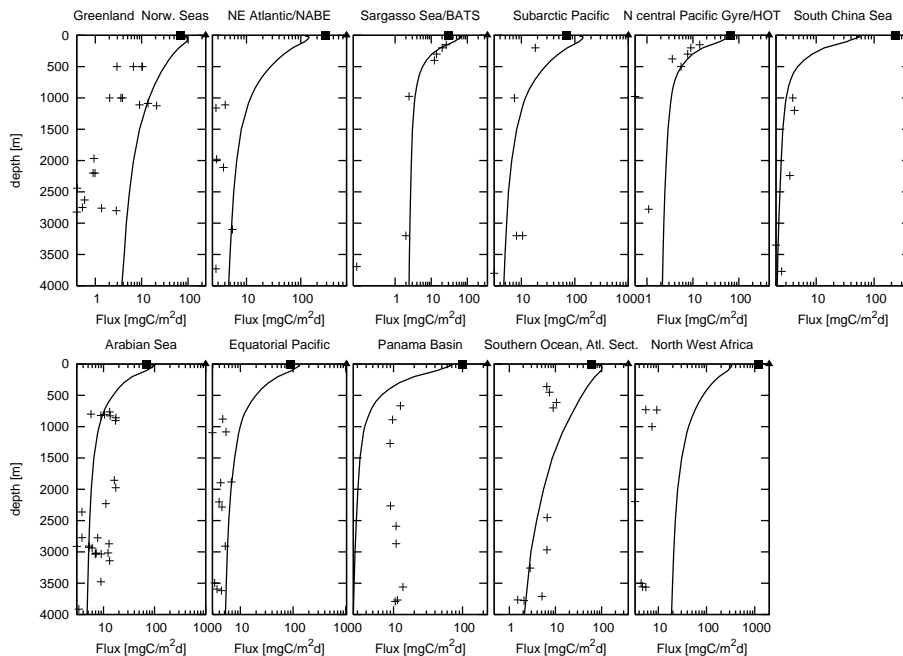


**Figure 8.** The flux of organic carbon in 11 regions. This model (solid line) and data (symbols) from Lutz et al. (2002). The model reaches steady state at about 5–10 years. We run two instances of each experiment for 18 years and take the mean of the last 4 years of the two runs.

## Sinking aggregates

T. Jokulsdottir and  
D. Archer

Title Page

Abstract

Introduction

Conclusions

References

Tables

Figures

◀

▶

◀

▶

Back

Close

Full Screen / Esc

Printer-friendly Version

Interactive Discussion

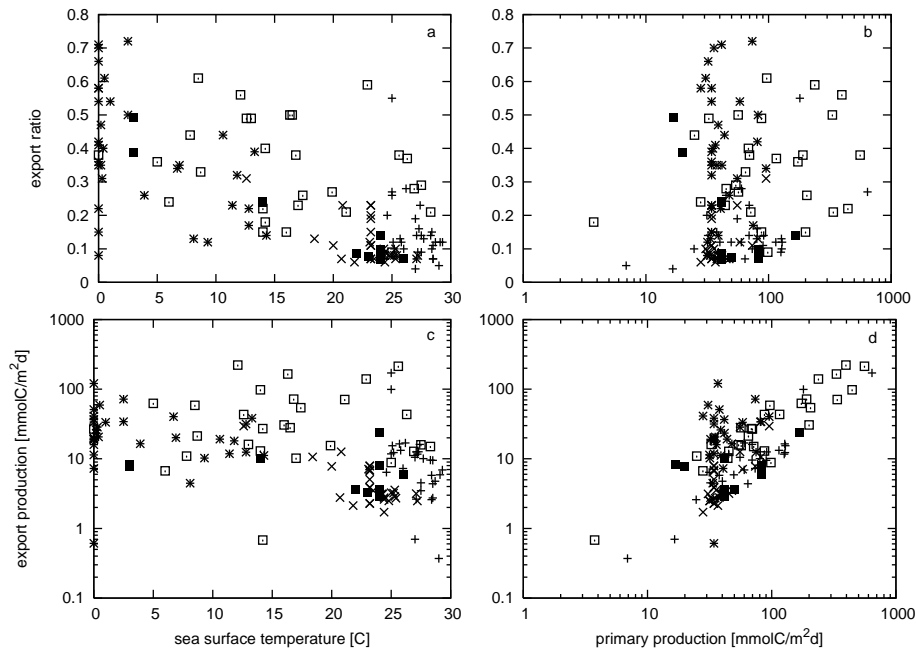


**Figure 9.** Model-data comparison of the export-ratio (the fraction of produced organic carbon that is exported) as a function of SST (a) and PP (b) in tropical (plus signs), subtropical (crosses), subpolar (stars) and coastal (open squares) regions; model-data comparison of the export production (in  $\text{mmolC m}^{-2} \text{d}^{-1}$ ) as a function of SST (c) and PP (d). Model results (solid squares) are from the 11 regions listed in Table 3, data from Dunne et al. (2005).

## Sinking aggregates

T. Jokulsdottir and  
D. Archer

Title Page

Abstract

Introduction

Conclusions

References

Tables

Figures



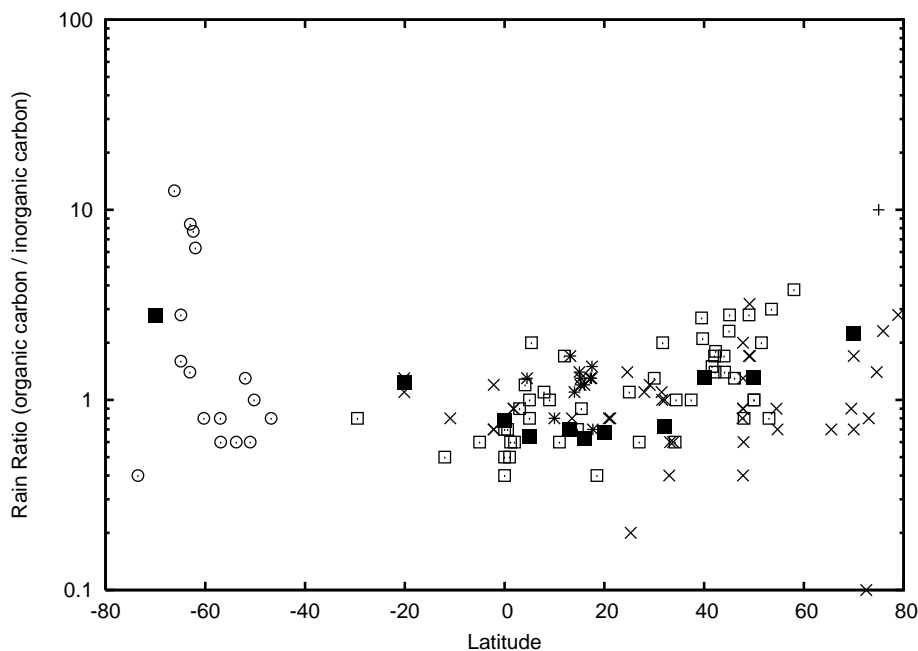
Back

Close

Full Screen / Esc

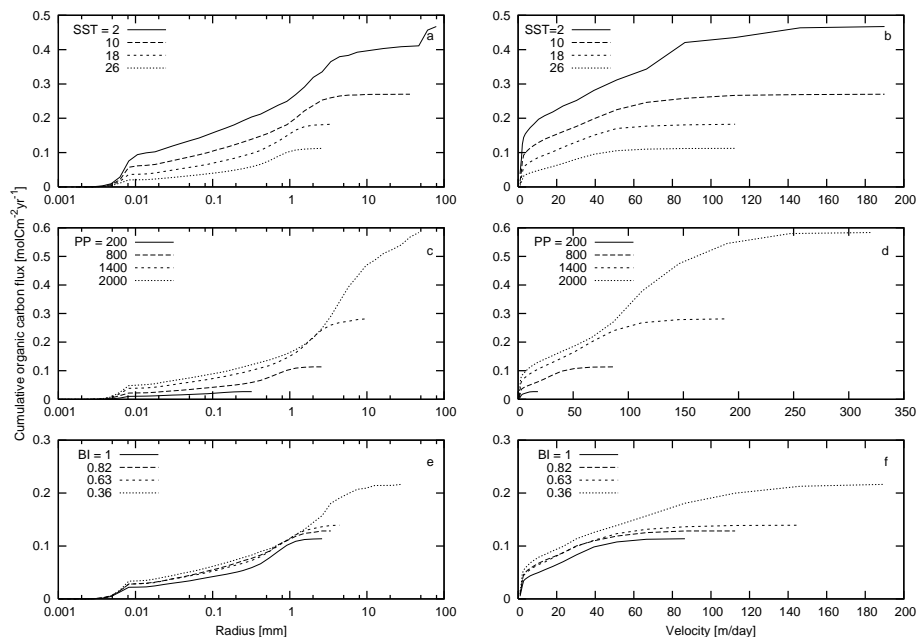
Printer-friendly Version

Interactive Discussion



**Figure 10.** The rain ratio (organic carbon to inorganic carbon) of material reaching the seafloor as a function of latitude. Data from the Southern Ocean (circles), Pacific Ocean (open squares), Indian Ocean (stars), Atlantic Ocean (crosses) and Arctic Ocean (plus sign) (Data from Honjo et al., 2008). Model results (solid squares) for the 11 regions mentioned above.

## Sinking aggregates

T. Jokulsdottir and  
D. Archer

**Figure 11.** Cumulative flux of organic carbon reaching the seafloor (4 km) as a function of aggregate radius and velocity for varying sea surface temperatures (**a, b**), primary production (**c, d**) and bloom index (**e, f**). Default SST = 24 °C, PP = 1000 mgCm<sup>-2</sup>d<sup>-1</sup> and bloom index = 1.

Title Page

Abstract

Introduction

Conclusions

References

Tables

Figures

◀

▶

◀

▶

Back

Close

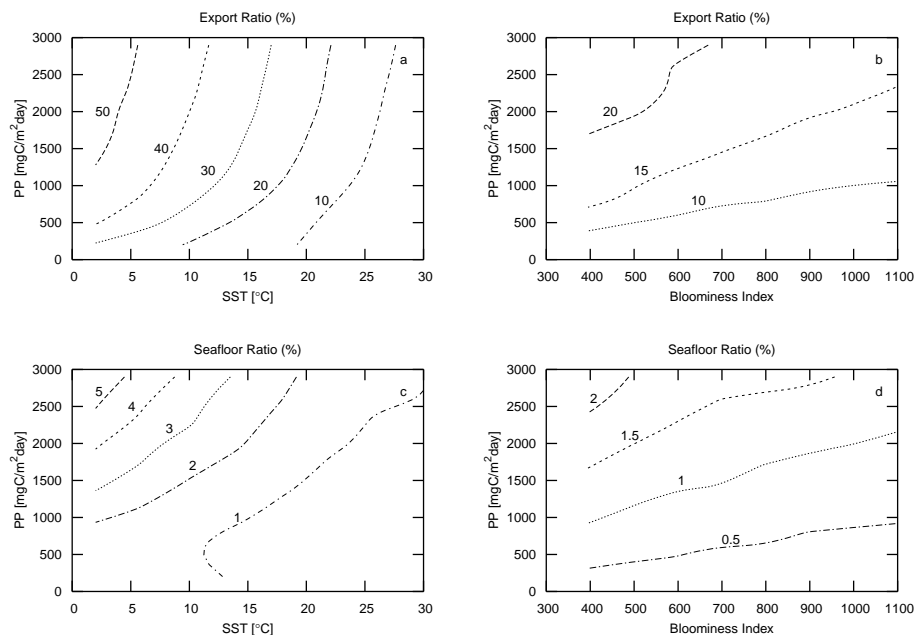
Full Screen / Esc

Printer-friendly Version

Interactive Discussion



## Sinking aggregates

T. Jokulsdottir and  
D. Archer

**Figure 12.** Export ratio (in %) (**a, b**) and percentage of primary production that reaches 4 km depth – Seafloor Ratio (**c, d**) as a function of primary production and sea surface temperatures (**a, c**) and bloom index (**b, d**). Numbers represent flux as a percentage of primary production.

Title Page

Abstract

Introduction

Conclusions

References

Tables

Figures

◀

▶

◀

▶

Back

Close

Full Screen / Esc

Printer-friendly Version

Interactive Discussion

